END
DATE
FILMED
3 84
DTIC

MICROCOPY RESOLUTION TEST CHART
NATIONAL BUREAU OF STANDARDS-1963-A

AD

ANNUAL

PROGRESS REPORT

for

U.S. ARMY MEDICAL RESEARCH AND DEVELOPMENT COMMAND
Fort Detrick, Frederick, Maryland 21701

from

RC-RCS-036
The Johns Hopkins University
Applied Physics Laboratory
Johns Hopkins Road
Laurel, Maryland 20707

on

A STUDY OF LOW LEVEL LASER RETINAL DAMAGE

Approved for public release; distribution unlimited.

B. F. Hochheimer

February 1, 1984

DTIC
ELECTE
FEB 0 9 1984
E

84 02 09 010

AD

ANNUAL

PROGRESS REPORT

for

U.S. ARMY MEDICAL RESEARCH AND DEVELOPMENT COMMAND
Fort Detrick, Frederick, Maryland 21701

from

RC-RCS-036
The Johns Hopkins University
Applied Physics Laboratory
Johns Hopkins Road
Laurel, Maryland 20707

on

A STUDY OF LOW LEVEL LASER RETINAL DAMAGE

B. F. Hochheimer

February 1, 1984

REPORT DOCUMENTATION PAGE		READ INSTRUCTIONS BEFORE COMPLETING FORM
1. REPORT NUMBER RC-RCS-036	2. GOVT ACCESSION NO. AD-A137664	3. RECIPIENT'S CATALOG NUMBER
4. TITLE (and Subtitle) A Study of Low Level Laser Retinal Damage		5. TYPE OF REPORT & PERIOD COVERED Annual Progress Report 2/1/83-1/31/84
		6. PERFORMING ORG. REPORT NUMBER
7. AUTHOR(s) Bernard F. Hochheimer		8. CONTRACT OR GRANT NUMBER(s) N00024-83-C-5301
9. PERFORMING ORGANIZATION NAME AND ADDRESS The Johns Hopkins University Applied Physics Laboratory Johns Hopkins Road, Laurel, Maryland 20707		10. PROGRAM ELEMENT, PROJECT, TASK AREA & WORK UNIT NUMBERS
11. CONTROLLING OFFICE NAME AND ADDRESS U.S. Army Medical Research & Development Command Fort Detrick, Maryland		12. REPORT DATE February 1, 1984
		13. NUMBER OF PAGES 55
14. MONITORING AGENCY NAME & ADDRESS(If different from Controlling Office) Non-Ionizing Radiation Division Letterman Army Institute of Research Presidio of San Francisco, California 94129		15. SECURITY CLASS. (of this report) Unclassified
		15a. DECLASSIFICATION/DOWNGRADING SCHEDULE

16. DISTRIBUTION STATEMENT (of this Report)

Approved for public release; distribution unlimited.

17. DISTRIBUTION STATEMENT (of the abstract entered in Block 20, if different from Report)

18. SUPPLEMENTARY NOTES

19. KEY WORDS (Continue on reverse side if necessary and identify by block number)

Laser Retinal Damage

20. ABSTRACT (Continue on reverse side if necessary and identify by block number)

The general objective of this program is to document changes in the retina due to very low laser irradiation. We have two primary aims. One is to develop and improve methods that can be used, in vivo, to objectively determine changes that occur in the retina from laser irradiation. The second is to determine the mechanisms that cause these retinal changes.

During this past year we have:

DD FORM 1473 EDITION OF 1 NOV 65 IS OBSOLETE
1 JAN 73

(1) Measured the change in retinal reflectivity during YAG and Argon Ion laser burn periods.

(2) Determined the fluorescence decay time of fluorescein dye in water, blood and monkey retinas.

(3) Obtained estimates of the amount of scattered light in the eye in the green and red spectral regions.

DISTRIBUTION:

Commander
U.S. Army Medical Research and Development Command
ATTN: SGRD-RMS
Fort Detrick, Frederick, Maryland 21701
4 copies

Defense Documentation Center (DDC)
ATTN: DDC-TCA
Cameron Station
Alexandria, Virginia 22314
12 copies

Superintendent
Academy of Health Sciences, U.S. Army
Fort Sam Houston, Texas 78234
1 copy

Dean, School of Medicine
Uniformed Services University of Health Sciences
Office of the Secretary of Defense
4301 Jones Bridge Road
Bethesda, Maryland 20014
1 copy

Commander
Letterman Army Institute of Research
ATTN: SGRD-ULZ-RCM/Dr. Neville
Presidio of San Francisco, California 94129
6 copies

FORWARD

In conducting the research described in this
report, the investigator(s) adhered to the "Guide for
Laboratory Animal Facilities and Care," as promulgated
by the Committee on the Guide for Laboratory Animal,
Resources, National Academy of Sciences-National
Research Council.

TABLE OF CONTENTS

Title   Page

CHANGES IN RETINAL REFLECTIVITY DUE TO A LASER BURN

Introduction

The objectives of this part of the program are:

1. To detect and quantify the subtle clouding effect seen at the retina with low level gallium arsenide laser irradiation.

2. To determine if measurements of retinal reflectivity during laser irradiation will aid in an understanding of low level laser damage mechanisms.

3. To determine the optimum wavelength(s) to use to detect laser retinal damage several days to months after the damage has occurred.

Methods

A modified fundus camera is used to illuminate a small area of the retina with light from a fiber optics light source. Energy from either a YAG or Argon Ion laser is introduced into the light collection optics by a dichroic beam splitter. The laser light goes through the camera focusing lenses and is sharply imaged on the retina at the center of the fiber optics illuminated area. The reflected energy from the retina is imaged at an iris diaphram which is located at the retinal image over the same area as the fiber optics source. Light going from the aperture goes through a rotating variable wavelength interference filter monochromator and then to a S-20 response photomultiplier tube. The PMT signal is amplified by a digital voltmeter. Data is collected and analyzed by a HP9845B computer. The computer also controls a stepper motor which rotates the filter monochromator.

With this system, a reflection spectra of the retina can be recorded at 20 wavelengths from 400 to 1200 nm in 5.3 seconds. The S-20 PMT has little sensitivity above 800 nm but can be replaced with a S-1 response tube if it is desirable. It is also possible to pulse the laser on and off and record reflection data only when the laser is off.

Results

A. YAG Laser Burns

In Table I are shown the results from five YAG laser burn measurements of retinal reflectivity. The CW YAG laser power at the cornea is approximately 50 milliwatts multimode. Tests 1, 3 and 5 were made with full intensity; Test 2 with a neutral density filter of 0.15 in the laser beam; and Test 5 with a 0.3 neutral density filter. In Test 5, no laser burn could be

TABLE I

1. Laser on 121 Seconds, Full Intensity

λ	% Increase in retinal reflectivity
462	78
540	70
658	60
695	53

2. Laser on 303 Seconds, Full Intensity with ND 0.15

λ	% Increase in retinal reflectivity
462	22
540	28
658	16
695	22

3. Laser on 191 Seconds, Full Intensity (Graphs are shown for this data)
    (Laser on 63 to 254 seconds)

λ	% Increase in retinal reflectivity
462	92
540	107
658	67
695	48

4. Laser on 300 Seconds, Full Intensity

λ	% Increase in retinal reflectivity
462	116
540	150
658	89
695	69

5. Laser on 307 Seconds, Full Intensity ND 0.3

    No change in any wavelength

seen; and there was no detectable change in retinal reflectivity at any
wavelength. Although the laser power level is not well known, a reduction in
power level by a factor of two will not produce ophthalmoscopically visible
retinal damage.

With full intensity, the reflectivity increases with an increase in irradiation time; and the greatest increase is at the shorter wavelengths. Data is not recorded past 700 nm because of a filter in the detector light path to remove the 1.06 micron laser energy. With the neutral density 0.15 filter, the increase in reflectivity is reduced by about a factor of five times from the full intensity burns (compare Test 2 and 4).

The data recordings for Test 3 are shown in Figure 1. One hundred and fifty spectral scans were recorded with a ten second delay between scans. Our computer storage limits the total number of scans to less than 200 so that even though a single scan takes only 5.3 seconds a time delay between scans is necessary if a long recording time is desirable. The laser was turned on from 63 to 254 seconds, a 191 second burn period. An inspection of the curves in Figure 1 shows that the retinal reflectivity did not increase until approximately 100 seconds, that is 40 seconds after the laser was turned on. The peak increase in reflectivity occurs at approximately 250 seconds, the time the laser was turned off. From that time until the end of the test, 2370 seconds, almost 40 minutes, there is a gradual decrease in reflectivity.

B.   Argon Ion Laser Burns

Argon ion laser retinal burns were made using the 488 nm line in a manner similar to that used for the YAG laser burns except that a 515 nm long pass filter was used in the detector light path to remove reflected laser light. Figure 2 is the first sheet from the computer. It records the initial data including the voltage signal levels and reflectivity of the standard reflector. The standard reflector is Kodak White Reflectance Standard and a neutral density 1.0 filter. Standard reflection signals of less than 0.045 are due to residual dark current in the PMT. The time at the end of each scan is recorded. The number after the scan time is the voltage recorded for 500 nm; this is used as a check on system performance during a test. Table II shows the wavelengths at which data is recorded. For the test run indicated in Figure 2, the laser was on from 26.5 to 111.3 seconds at a power level sufficient to produce a definite burn. The wavelength data is plotted as shown in Figure 3A. The data point at 200 units is the cross over from one half of the interference monochromator to the other half and not a good point. Figure 3B is at 106 seconds when the laser is on and indicates a high degree of retinal fluorescence. Figures 4A and 4B are after the laser was turned off. Specific wavelength data is plotted as shown in Figures 5 and 6. Figure 5A is at 462 nm and not useful because of the 515 nm long pass filter. Figure 5B shows the data at 540 nm. Before the laser is turned on, the retinal reflectivity is approximately 11 percent; during the laser burn, the fluorescence swamps out the signal; after the laser burn, the reflectivity has risen to 17 percent and slowly decreases to 15 percent at 1000 seconds after the burn. Figure 6 shows similar data for 658 and 760 nm.

We can also pulse the laser on and off with a Uniblitz shutter and record reflectance data when the laser is off thereby avoiding the fluorescence problem. In the previous continuous maximum power test, the laser was on for 85 seconds. In a series of pulse tests, the laser was on for 90 seconds in 1.8 second bursts every 5.4 seconds. The data is similar at high power to the continuous burns. With the laser power level reduced by 25

TABLE II

Data Point Number	Wavelength nm	Standard Signal level, volts	
1	345	0.04087	⎫
2	384	0.04372	⎬ NG
3	423	0.04846	⎭
4	462	0.05099	
5	501	0.10528	
6	540	0.93819	
7	579	0.98578	
8	618	0.93477	
9	658	0.82208	
10	697	0.55451	
11	NG	0.05101	NG
12	757	1.09997	
13	820	0.29215	
14	882	0.06659	⎫ ?
15	940	0.04281	⎭
16	1002	0.04667	⎫
17	1065	0.04202	⎬ NG
18	1127	0.04061	
19	1190	0.04363	
20	345	0.04511	⎭

times, pulsed mode, the data in Figure 7 was recorded. The 515 nm long pass filter was removed. At 462, 540, 658 and 695 nm, a slight rise in reflectivity can be detected. The laser pulse time was from 21.3 to 467 seconds.

We also plot the data from a given scan minus the average value up to that time. This type of plot shows the trend of the data; if the trend is positive, the values are increasing. In general, the trend plots, Figure 8, show a constantly increasing reflectivity. At 540 nm, the increase is small near 200 seconds; but it is still positive. At 695 nm, the increase is approximately zero until after 200 seconds when it increases. These curves show that although the initial and final values are almost identical for all wavelengths these values are not arrived at in the same way.

This pulsed energy did not produce a retinal burn visible immediately after the test, but one was just visible one hour later. A change in reflectivity could be recorded at the time when a burn could not yet be seen.

This test produced 200 spectral scans, the data for all wavelengths is printed out for every fifth scan as shown in Figure 9. The first row of numbers is the scan number, the second row the reflectivity at λ_1, the third row at λ_2, etc. This order is repeated for every set of numbers. As an example, the fifth row of numbers in the first set are the

reflectivity values for 462 nm. The initial value is 8.5 percent; it rises to 10.2 percent at the 71st scan, decreases somewhat for scans 101 to 126 and gradually rises to 10.5 percent at scan 196.

C.   Retinal Fluorescence

As noted above, we found a high degree of retinal fluorescence. Since all of our monkeys have had one or more fluorescein angiograms, we do not know if the fluorescence is due to residual fluorescein.

The spectra of this retinal fluorescence due to 488 nm laser light was recorded with continuous illumination. The 515 nm long pass filter was used to remove the laser light; this distorts the spectral shape of the fluorescence.

Figure 10 is the recorded spectra; the Y-axis should read relative intensity. No correction for instrument transmission is included. Taking into consideration the influence of the 515 nm filter, this spectra could be due to fluorescein.

Figure 11 is the time history of the fluorescence for 462, 540, 658 and 695 nm. Because of the filter, there is no energy at 462 nm. In the remaining time histories, there is a rapid rise in fluorescence to a peak value, a rapid decay and a slow decay to a constant value. The high peak rise seems to disappear if the retina is not burned. In this case, the signal to noise ratio in the recorded energy values is low; therefore, there is some uncertainty in this. In Figure 11, the dotted curves are the originally recorded data, and the solid curves are running averages over five points.

D.   Photographic Records

One eye of a monkey had a series of eight burns placed on his retina with the 488 nm line of the Argon Ion laser. Power levels were varied over a factor of 25 times in making these burns. Fundus photographs were taken at 450 to 850 nm in 50 nm steps at various times after retinal exposure. This series and the times after exposure are shown in Figure 12. The retinal burns are most apparent at short wavelengths immediately after exposure and at red (600-650 nm) several days later. At no time are they most visible in the near infrared.

Problem Areas

A.   Locating Old Burns

We wished to photoelectrically record the reflectivity of the retina at laser burn areas for long post-irradiation times. Unless the burn is very severe, a healing process takes place; and we can no longer see the

- 5 -

burns with our fundus camera. Since the laser retinal burns are very small, approximately 50 microns in diameter, the fiber optics illumination used for reflectivity measurements must be positioned with high accuracy. This cannot be done unless the burns can be seen. Because of this, the reflectivity can not be measured at long post-exposure times.

B.   Computer Data Collection

One of the problems in using a computer to collect data is that there is often an overabundance of data. We have not yet had enough time to analyze all of our retinal reflectivity data. A second unresolved problem is the proper format to display the results. We are getting better at this.

C.   Equipment Reliability

As our experiments are becoming more sophisticated, the equipment used is more complex. For many of our tests, we could not measure the laser power at the eye because our Laser Precision Power Meter was being repaired. During the past year, the Princeton Applied Research signal averager and the Hewlett-Packard computer have needed factory repairs. The Hewlett-Packard multiprogrammer used to operate stepper motors and do analog to digital conversion is now at the factory for repair. Because of this problem, we are making redundant measurements as often as possible.

Conclusions

1.   Changes in retinal reflectivity can be detected photoelectrically at levels below those that can be observed visually.

2.   With continuous wave YAG laser energy, it is difficult to observe near threshold retinal lesions because the energy difference necessary to make a highly visible burn and that which will make no burn is very small.

3.   For detection of old retinal laser-induced lesions, a monochromatic series of retinal photographs covering the range from 400 to 800 nm is the method we recommend. This question will be considered further in the section on future efforts.

4.   I have replotted the data for the pulsed Argon Ion laser test shown in Figure 9. The retinal reflectivity is plotted in Figure 13 to show the increase with time and wavelength. Plotted is data for the 1st scan, before irradiation; the 61st scan, almost at the end of the irradiation period; and the 196th scan, at the end of the data collection period.

There is a rather constant increase in reflectivity at all wavelengths shorter than 800 nm. The data at 882 is plotted but

- 6 -

may not be reliable. If it is assumed that different retinal layers can be seen with variations in wavelength, deeper layers are seen at longer wavelengths, then this plot might indicate that all layers of the retina above the choriocapillaries are being equally damaged. I think it is more likely that the pigment epithelium is being damaged and there is a white layer of edema formed that is transparent at 800 nm.

Measurement of Scattered Light

In last year's progress report, we showed that if a very small area of the retina is directly illuminated the total amount of light impinging on the rest of the retina may be between one-half to over ten times the directly illuminated power. A small area of retina was illuminated, and the directly reflected light was compared to the light coming from a similar area of the retina some distance away from the directly illuminated area. In the visible spectral region, the nonilluminated area at six degrees from the illuminated area reflected approximately 1/500 of the energy from the illuminated area. At 750 nm, this ratio is 1/50 and at 800 nm 1/10. In the visible spectrum, our data agrees very well with other published data. The ratio of illuminated area to nonilluminated area of the retina was approximately 10^{-4}.

This stray light in the eye is composed of light scattered by the cornea, aqueous, lens and vitreous; by light reflected many times by the retina; and by light internally scattered in the choroid and sclera. An expression for the reflected light term was derived using simple geometry and assuming a diffuse retina. The derived expression indicated that only a very small amount of light should be internally reflected even for very high values of retinal reflectivity. Even if the retina is 100 percent reflecting, the internal reflected energy per unit area would only approach the ratio of illuminated to nonilluminated area.

From our experiments that measured the increase in reflectivity of the retina when it is burned with a high energy laser beam, we knew that the retinal reflectivity could be increased by almost a factor of two for wavelengths from 500 to 800 nm. Using this fact, we can deduce some information on the percentage of light scattered in the eye.

If the retinal reflectivity is R_1 for a nonburned area, R_2 for a burned area and the amount of scattered light is S, then the directly reflected energy E measured from nonburned area is

$$E_1 = KR_1(1 - S)^2 \qquad (1)$$

where K is a nondefined constant. The directly reflected energy measured from the burned area is

$$E_2 = KR_2(1 - S)^2. \qquad (2)$$

The ratio of these terms is

$$\frac{E_1}{E_2} = \frac{R_1}{R_2}. \qquad (3)$$

For a nonilluminated area some distance from the laser burn when the burned area is illuminated, the measured reflected energy before the burn will be

$$E_1{}^1 = K\left(\frac{A}{s}\frac{R_1}{(1-Y)}(1-S)^2 + \frac{A}{s}\frac{S(1-S)}{(1-Y)}\right). \qquad (4)$$

A/s is the ratio of illuminated to nonilluminated area, Y the area weighted reflectivity and R and S are defined as above. This expression and its derivation is similar to that in last year's progress report with an additional scattering term $S(1-S)/(1-Y)$.

When the illuminated area is burned with a laser, its reflectivity will increase, increasing the measured scattered light to a value given by

$$E_2{}^1 = K\left(\frac{A}{s}\frac{R_2}{(1-Y)}(1-S)^2 + \frac{A}{s}\frac{S(1-S)}{(1-Y)}\right). \qquad (5)$$

The ratio of equations (4) to (5) is

$$\frac{E_1{}^1}{E_2{}^1} = \frac{R_1(1-S)+S}{R_2(1-S)+S}.$$

Let

$$\frac{E_1}{E_2} = \frac{1}{C_1} = \frac{R_1}{R_2}$$

or

$$R_2 = C_1 R_1$$

and

$$\frac{E_1{}^1}{E_2{}^1} = \frac{1}{C_2}$$

then

$$\frac{1}{C_2} = \frac{R_1(1-S)+S}{C_1 R_1(1-S)+S}.$$

C_1 and C_2 are measured energy ratios on and off the burned areas. Let $R_1 = R$, the retinal reflectivity before being laser burned. S is the amount of scattered light, $(1-S)$ the energy not scattered that reaches the retina.

Rearranging the terms

$$C_2 R(1-S) + C_2 S = C_1 R(1-S) + S$$

$$C_2 S - C_2 RS + C_1 RS - S = C_1 R - C_2 R$$

- 9 -

$$S = \frac{R(C_1 - C_2)}{(C_2 - 1) + R(C_1 - C_2)}.$$

If C_1, C_2 and R are known, S can be found.

Using the same optical system described in the section on Retinal Reflectivity, three burns were placed on the retina of a cynomolgus monkey in the region above the macula using the 488 nm line of an argon ion laser for 90 seconds. Although the amount of laser energy is unknown, it was kept at a constant value and the burn time fixed at 90 sec with a Uniblitz shutter. The area to be burned was illuminated with white light. The reflected energy was filtered first with a 515 nm long pass filter to eliminate the laser energy and secondly with a variable wavelength interference filter monochrometer whose bandwidth is 20 nm.

The monochrometer was set at 550 nm, and the reflected energy measured before and after the laser burn. The area used for energy measurements was about one-half the diameter of the laser burn.

The measured values of C_1, the energy ratios after the burn to before the burn, are 1.95, 2.40 and 3.04. The reflected light from an area three degrees away from the burn area was then measured for a second set of burns. This second set of burns were just below the first set. The measured values of C_2 are 1.19, 1.50 and 1.52. It is apparent that the repeatability is not high.

Similar sets of burns were made with the monochrometer set at 650 and 750 nm. There is insufficient energy to do this at 800 nm. The results are tabulated in Table I.

These values were averaged and values of $(C_1 - C_2)$ and $(C_2 - 1)$ computed. Using what seems to be an appropriate value for retinal reflectivity, the amount of scattered light was found. This is shown in Table II. Values of S were also calculated for higher values of R.

Over this past year, many measurements have been made of the retinal reflectivity of cynomologus monkeys. Using what I believe to be our most reliable sets of data, the reflectivity at 550, 650 and 750 nm were obtained and are listed in Table III.

If the scattered light is as high as it appears to be, the measured values of retinal reflectivity are too low; they should be increased by $1/(1 - S)^2$ where S is taken at a true value of R.

Since our accuracy is not high, one iteration is sufficient. I believe this exercise indicates that the scattered light (cornea-lens-vitreous-aqueous) is high in the visible spectral region 30-40 percent and decreases in the red to 10 percent and that the retinal reflectivity is higher than previously estimated.

This scattering would account for the large value of stray light in the visible but not in the infrared. Since the amount of internally reflected

TABLE I

$\lambda = 550$ nm	C_1	C_2
	1.95	1.19
	2.40	1.50
	3.04	1.52

$\lambda = 650$ nm	C_1	C_2
	2.36	1.43
	2.36	1.31
	2.38	1.46

$\lambda = 750$ nm	C_1	C_2
	1.65	1.33
	1.49	1.36
	1.65	1.50

TABLE II

$\lambda = 550$ nm $C_1 - C_2 = 1.1$

         $C_2 - 1 = 0.40$

R = 10%	R = 20%	R = 40%
S = 21%	S = 36%	S = 52%

$\lambda = 650$ nm $C_1 - C_2 = 0.97$

         $C_2 - 1 = 0.40$

R = 15%	R = 30%	R = 60%
S = 26%	S = 42%	S = 59%

$\lambda = 750$ nm $C_1 - C_2 = 0.20$

         $C_2 - 1 = 0.40$

R = 20%	R = 40%	R = 80%
S = 9%	S = 17%	S = 28%

light is probably low at all wavelengths, the high value of stray light in the red and infrared must be due to light scattered by the choroid and sclera.

Geeraets and Berry (AJO 66, 15, 1968) give spectral absorption curves for monkeys and humans. The monkeys used were rhesus, the cynomolgus we use are much less pigmented. The human data may be more appropriate.

TABLE III

	550 nm	650 nm	750 nm
	0.14	0.18	0.26
	0.08	0.12	0.20
	0.10	0.17	0.25
	0.11	0.17	0.24
	0.10	0.14	0.19
Average	0.106	0.156	0.228

TABLE IV

λ	550 nm	650 nm	750 nm
Measured R	10%	15%	20%
Computed S	21%	26%	9%
$(\frac{1}{1-S})^2$	1.6	1.8	1.2
$R(\frac{1}{1-S})^2$	16%	27%	24%
New computed S	31%	40%	11%

TABLE V

λ nm	% Absorption	$(Transmission)^2$
550	75	0.06
650	65	0.12
750	45	0.30
800	35	0.42

When light hits the choroid, some is transmitted, is reflected by the sclera, is transmitted back through the choroid. If it is assumed that the sclera is almost 100 percent reflecting, then in the red 30 to 40 percent of the light impinging on the retina may be reflected back into the eye.

Table VI is a comparison between our data taken on live monkey eye and the data of Geeraets and Berry for the retinal reflectivity of an enucleated human retina and the data of Boettner and Wolter (Invest. Opthal., 1,776, 1962). These data were taken with different eyes and even different species yet the agreement is fairly good. Our data for scattered light at 650 nm

TABLE VI

| λ | Our Data | | Geeraets & Berry | Boettner & Wolter |
	% Scattered Light	% Retinal Reflectivity	% Human Retinal Reflectivity	% Scattered Light Optics
550	30	16	12	35
650	40	27	17	30
750	10	24	22	26

seems to be too high; and since this also effects the reflectivity at that wavelength, it is also high.

Stray Light at Long Wavelengths

Our previous measurements were taken only at 50 nm intervals from 500 to 800 nm. We wished to both extend the wavelength region and to record data at smaller intervals. In order to do this, we used a two-channel signal averager. White light from our fiber optics source illuminated a small retinal area. The return beam went through a free running rotating interference filter monochrometer. The directly reflected light was stored in channel B and the reflected light three degrees away was stored in channel A. Using an S20 response photomultiplier tube, data was taken from 450 to 825 nm. The ratio of channel A to channel B is the percentage of stray light from the retina corrected for input energy and instrument reponse. This method is excellent for indicating the whole spectral variation; however, many scans are needed for recording the indirectly reflected energy, and long-term drift in DC levels prevent recording absolute values. In addition to this, a zero-level error can produce an unknown tilt in the zero axis. Figure 14 shows the A and B scan and the A/B ratio. In Figure 14, our best estimate of the zero x-axis for the A/B ratio is drawn in. The stray light increases at short wavelengths, shows some structure between 450 and 500 nm, is almost flat to 700 nm and rises quickly from 700 to 825 nm. This is what is expected based on last year's data.

The S20 PMT was replaced with an S1 tube, and the experiment was repeated for the range from 700 to 950 nm. Figure 15 are two A/B ratios using 20 scans. These curves indicate a rapid rise after 700 nm and a level value to 950 nm. In order to determine if the fine structure in these curves are real, a 200 scan recording was made; see Figure 16. The fine structure disappears with sufficient averaging to remove noise.

Summary

Although much of the data we have obtained this year has low accuracy, it has enabled us to get a much better overall picture of stray light in the

eye. In the visible, the stray light is lowest and almost entirely due to light scattered by the optics of the eye. In the red and near infrared, the scattering decreases but the energy transmitted through the choroid and reflected by the sclera predominates. At all wavelengths, light reflected by the retina, as if the eye acted like an integrating sphere, is negligible.

This stray light does not affect our visual acuity because most of the stray light strikes the retina at high angles of incidence and is very inefficient in evoking any visual response. The Stiles and Crawford effect (B. H. Crawford, Proc. of the Royal Soc., 124, 81, 1938) indicate that light hitting the retina 14 degrees off axis has an efficiency of only 10 percent of that on axis; and the efficiency is falling fast, even on a log plot, for larger angles.

FLUORESCEIN DYE FLUORESCENCE

Introduction

The rate of emission of fluorescent light is given by

$$E = I_a \phi_f$$

where I_a = absorbed light

and ϕ_f = fluorescence efficiency and is given by

$$\phi_f = K_f/(K_f + K_n + K_g + K_q(Q))$$

where K_f = fluorescence rate constant

K_n = nonradiative rate constant

K_g = triplet state formation rate constant

K_q = quenching rate constant, a function of the amount of quencher (Q).

When the light is turned off, the fluorescence decays with a lifetime τ where τ is given by

$$1/\tau = K_f + K_n + K_g + K_q(Q)$$

let τ_f = radiative lifetime

if $1/\tau_f = K_f$

then $\phi_f = \tau/\tau_f$.

If τ_0 is the lifetime with no quencher and ϕ_f^0 the efficiency with no quencher, then

$$\tau_0 = 1/\phi_f^0 = 1/(K_f + K_n + K_g)$$

and

$$\phi_f^0/\phi_f = 1 + K_q(Q)/(K_f + K_n + K_g) = 1 + K(Q)$$

where K is generally known as the Stern-Volmer quenching constant or

$$\phi_f^0/\phi_f - 1 = K_q \tau_0 [Q] = K(Q);$$

the quenching is given by ϕ_f/ϕ_f^0 or τ_0/τ_f

$$\text{quenching} = 1/(K(Q) + 1) = 1/(K_q \tau_0(Q) + 1).$$

If the quencher is oxygen, then

$$(Q) = Sp O_2$$

where S is the solubility and pO_2 the partial pressure of oxygen. K_q is
dependent on viscosity (C. A. Parker, PHOTOLUMINESCENCE OF SOLUTIONS, Elsevier
Publishing Co., New York, 1968).

In most solutions, oxygen is a very efficient quencher by transfer of
triplet state dye energy to the triplet ground state of oxygen forming excited
singlet oxygen and a ground state dye molecule. The reaction is diffusion
limited and hence the dependence of K_q on viscosity. It is possible to
determine the degree of quenching by measuring either the intensity loss or a
change in decay time. An intensity loss may also occur if a dye molecule is
bound to another molecule with an increase in the nonradiative losses.

We know that the fluorescence intensity of fluorescein in blood is lower
than in water by approximately two times. A pyrene dye, which absorbs and
fluoresces at the same wavelength as fluorescein, does not show the drop in
intensity in blood compared to water (Hochheimer, Exp. Eye Res. 27, 1,
1978). This indicates that blood contains a quencher for fluorescein and the
loss in intensity is not due to the absorption of light in blood. This
quenching effect for fluorescein can be due to the binding of dye to blood
proteins with an increase in nonradiative loss of the excited state or a
transfer of energy from the excited state to a second molecule. If the second
method predominates, oxygen may be the acceptor molecule.

The most common method used today to measure fluorescence decay times is
to use a fast pulse of excitation light and measure the decay of fluorescence
directly. If the decay time is not single valued, this method can detect
multiple decay times. The modulation-phase detection method that we use
assumes a single valued decay time. With the pulse method, high powered
pulses must be used; with the modulation method, low average energy can be
used. Since the retina is very sensitive to damage from nanosecond pulses of
light, we choose to use the modulation-phase shift method.

Method

In the eye, it is not possible to measure the fluorescence quantum
efficiency of a dye; however, it is possible to measure the fluorescence decay
time. To do this, the following system was assembled.

A Coherent Radiation Inova 90 Argon Ion Laser emits the 488 nm
transition. The laser beam is modulated by an Interacton AOM125H Acoustic-
Optic Modulator. The modulator is driven at 20 MHz by an Interacton ME Signal
Processor and a Hewlett-Packard 3325A Synthesizer/Function Generator. The
moldulated beam laser beam goes through our modified Zeias Fundus Camera to
either an animal eye or to a test solution. The fluorescent energy is
gathered by the fundus camera optics to an S-20 photomultiplier tube. A
Schott 515 nm long pass solid glass filter prevents the laser light from
reaching the PMT.

The output of the PMT is amplified by a Princeton Applied Research 5202 high frequency lock-in amplifier. This amplifier has a phase detector option which measures the in-phase and quadrature signals and computes both a phase signal and the signal amplitude. Both signals are recorded on a two-pen strip chart recorder.

If a modulated light beam excites a fluorescent dye, the fluorescence output is also modulated with a phase delay determined by the decay time. This phase shift ϕ is given by

$$\tan \phi = 2\pi f \tau$$

where f is the modulation frequency and τ the decay time (Bailey and Rollefson, J. Chem. Phys. 21, 1315, 1953). With a decay time of 10^{-8} seconds and a frequency of 20 MHz, the phase delay is approximately 45 degrees. The degree of modulation of the fluorescent energy decreases as the phase shift increases to zero at a 90 degree phase shift (Spencer and Weber, Ann. of N. Y. Acad. Sci. 158, 361, 1969). At 45 degrees, the phase shift is sensitive to changes in decay time without excessive loss in modulated fluorescence.

Results

We first measured the decay time in a fluorescein water solution, the fluorescein concentration was 5×10^{-5} molar. The measured decay time was 9.82×10^{-9} seconds. In order to obtain a zero phase reference signal, a white diffuse reflector is placed at the position of the fluorescein solution and the 515 nm filter removed.

Bailey and Rollefson measured the decay time at this concentration and found it to be about 7.0×10^{-9} seconds. In their experiment, the fluorescent energy was collected at 90 degrees to the excitation energy; in our experiment, the collected fluorescent energy is close to 0 degrees from the excitation energy. Multiple internal scattering in the solution would account for the difference. They also show the concentration dependence of the decay time. It varies from 4.6×10^{-9} seconds at low concentrations to 7.9×10^{-9} seconds at a concentration of 5×10^{-4} molar.

The water solution was replaced with a fluorscein-whole blood solution (monkey blood was used), the fluorescein concentration was 5×10^{-5} molar, assuming blood to have the same weight as water. Because of differences in weight between blood and water, because some of the fluorescein is bound and because blood contains solids, the molarity in blood is not well defined. The decay time in the fluorescein blood solution was measured to be 8.24×10^{-9} seconds.

A variable CO_2-O_2 gas mixture was injected over the fluorescein-blood solution as it was slowly stirred with a magnetic stirrer. Previous tests indicated that this procedure could be used to change the blood oxygen concentration without visibly changing the blood viscosity. There was no measured change in decay time upon going from 100 percent O_2 to 100 percent CO_2. Our system can easily detect a 0.1×10^{-9} second, the precision seems to be about 0.05×10^{-9} second. This result was quite a surprise; we had

expected a large change in decay time with oxygen concentration. There is a slight increase in fluorescein intensity with oxygenation, this is likely due to an increase in transmission.

We next injected a monkey with fluorescein and measured the decay time of the dye in the retina. This decay time did not seem to vary at times longer than several minutes after injection. In a normal nondamaged retinal area, the decay time was found to be 5.63×10^{-9} seconds; and on an area previously damaged by a laser, the decay time was 5.04×10^{-9} seconds.

A second monkey was given a fluorescein injection, and the fluorescent decay times measured when the animal was breathing pure oxygen and when the endotracheal tube was clamped off for three minutes forcing the animal to increase its CO_2 uptake. With 100 percent oxygen, the measured decay time was 5.31×10^{-9} seconds; and with the increased CO_2 breathing, it was 6.15×10^{-9} seconds.

Discussion

A comparison of some of the fluorescent properties of fluorescein when dissolved in blood and water seems to indicate conflicting evidence. There is a large decrease in intensity in blood. This could be accounted for by quenching reactions. The decay time, however, does not change dramatically nor does it change in blood with a change in pO_2. This lack of change in decay time indicates that some of the fluorescein dye molecules are bound in such a way that they no longer contribute to fluorescence. The nonfluorescent fluorescein molecules have either a very acid local environment, or the hydrogen atoms have been stripped away as in an alcoholic solution, or the dye structure is changed as in the change from fluorescein to nonfluorescing phenolphthalein. Either the remaining "nonbound" fluorescein molecules are shielded from O_2, or more likely, the O_2 is bound to the hemoglobin and the O_2 is shielded from the fluorescein.

The fact that blood has little effect on the decay time of fluorescein and is not affected by blood pO_2 means that any changes seen in the retina are probably not due to the fluorescein in the animal blood system.

The fluorescence decay time of fluorescein in an animal retina is much shorter than in blood and is even shorter than in a water solution. From previous experiments, the concentration of fluorescein in the retina at some twenty to forty minutes after injection seems to be about 5×10^{-5} molar based on the shape of the emission spectra and the local pH is about seven based on the shape of the excitation spectra. The decay time in the retina is also affected by the local oxygen concentration.

These retinal measurements can only be reconciled if there is a high degree of quenching, and the dye molecules are not bound as they are in blood. This is in agreement with fluorescence polarization data from the retina which indicates a low degree of binding.

When fluorescence measurements are taken on a burn-damaged area of the retina, the intensity increases, the polarization decreases and the decay time

decreases. I do not as yet have good excitation and emission spectra for this case.

The intensity and polarization changes indicate an increase of unbound dye; the decay time change indicates an increase in quenching. Any explanation of these changes that occur from a damaged to a nondamaged area of the retina would be very speculative without more information.

When the decay time measurements are incorporated in our main fluorescence program, then all the available fluorescent information can be obtained at the same time on the same animal for both normal and various degrees of light-damaged retina. This data together with the analysis of fluorescence in freeze-dried eyes should give us a better perspective of light damage in the eye.

FUTURE PLANS

1. Retinal reflection measurements will be made while the retina is being irradiated with a pulsed YAG laser. A transient effect can be seen where the retina appears white for a short period, 5-20 seconds, after the pulsed irradiation. This may be similar to the "clouding" of the retina seen by Lund and Beatrice with a pulsed gallium arsenide laser.

2. A long-term multi-wavelength series of retinal photographs will be made after continuous wave and pulsed YAG burns are made on a monkey retina. Lund (Supplement Invest. Ophth. and Vis. Sci., April 1974, p. 52) reported on a short-term photographic series of gallium arsenide laser burns. His results indicate a considerable difference exists between infrared laser burns and the burns we have documented for argon ion laser burns. We wish to have a longer term followup and do both CW and pulsed burns.

3. We have recently acquired a high brightness xenon arc source and the associated optics and animal holder that enables us to irradiate the retina with sufficient energy to cause a burn in reasonably short time at any wavelength from 400 to 1000 nm. From Ham's work (Ham, Mueller, Ruffolo, Cleary, Clark, Guerry and Guerry, "Biological Applications and Effects of Optical Masers," Army Research Report DADA 17-72-C-2177, 1982), we know the minimum intensity needed to make a retinal lesion in 100 seconds. The intensity will be doubled and 300 micron retinal lesions formed on a monkey retina at 50 nm intervals from 400 to 1000 nm. The time course of these lesions will be followed with monochromatic retinal photography at suitable intervals for the next six months to a year.

4. We will incorporate the fluorescence decay time measurements in our main fluorescence program so that all possible data can be collected from a single animal after one dye injection. Both normal and light-damaged retinal areas will be measured.

5. After a fluorescein dye injection, a monkey eye, with numerous light-induced retinal lesions, has been freeze dried and vacuum embedded with paraffin (Bellhorn, Invest. Ophthal. and Vis. Sci. 19, 870, 1980). These eyes will be sectioned and examined with fluorescence microscopy to determine where the fluorescein seen in angiograms is located.

6. Our analysis of light scatter in the eye is not completely satisfactory; further analysis is needed. We will repeat our previous measurements and then sacrifice the animal, enucleate the eye to obtain the retina and choroid for in-vitro measurements of reflectivity and transmission. Specular and diffuse reflectivity will be measured in-vivo and in-vitro, and scattered light will be measured in-vivo.

    All of our old data will be reviewed as well as our reference data; and with the new data, we hope to come to a satisfactory understanding of the problem of scattered light in the eye.

7. A monkey who has never had a fluorescein injection will have his retina irradiated with the 488 nm argon ion laser. The retinal fluorescence will be measured as the intensity is varied. We wish to know if the rapid rise to a high value is an indication of retinal damage. If it is, this indicates a change in molecular structure in the retina when a burn is made.

FIGURE CAPTIONS

Figure 1   Retinal reflectivity values taken during and shortly after a burn was made with a YAG laser.

Figure 2   First data sheet for an argon ion CW laser burn retinal reflectivity experiment.

Figure 3   Retinal reflectivity versus wavelength before and during an argon ion CW laser burn retinal reflectivity experiment.

Figure 4   Retinal reflectivity versus wavelength after an argon ion CW laser burn retinal reflectivity experiment.

Figure 5   Time history of retinal reflectivity for an argon ion CW laser burn retinal reflectivity experiment. Wavelengths 462, 540 nm.

Figure 6   Time history of retinal reflectivity for an argon ion CW laser burn retinal reflectivity experiment. Wavelengths 658, 760 nm.

Figure 7   Time history of retinal reflectivity for an argon ion pulsed laser burn retinal reflectivity experiment. Wavelengths 462, 540, 658, 695 nm.

Figure 8   "Trend" plots of time history of laser burns shown in Figure 7.

Figure 9   Retinal reflectivity data for every fifth wavelength scan for data plotted in Figure 7.

Figure 10   Fluorescence spectra of retina illuminated with 488 nm argon ion laser.

Figure 11   Time history of fluorescent energy at 462, 540, 658 and 695 nm.

Figure 12   Monochromatic light retinal photograph taken at various times after burns were made on the retina with an argon ion laser.

Figure 13   Changes in retinal reflectivity due to an argon ion laser burn.
            Scan 1, before burn
            Scan 61, at end of burn period, 470 seconds after start of
                experiment
            Scan 196, at 1100 seconds after start of experiment

Figure 14   A.   Retinal reflectivity at 3 degrees from illuminated area
            B.   Retinal reflectivity on illuminated area
            A/B   Ratio of energy reflected from nonilluminated to illuminated
                  retinal areas. 450-800 nm.
            Note: A and B are not corrected for intensity or instrument
            transmission.

Figure 15 Ratio of energy reflected from nonilluminated to illuminated
            retinal areas, 700-900 nm. 20 scans averaged.

Figure 16 Identical to Figure 15 except 200 scans averaged.

Maximum time is 2370.4 s
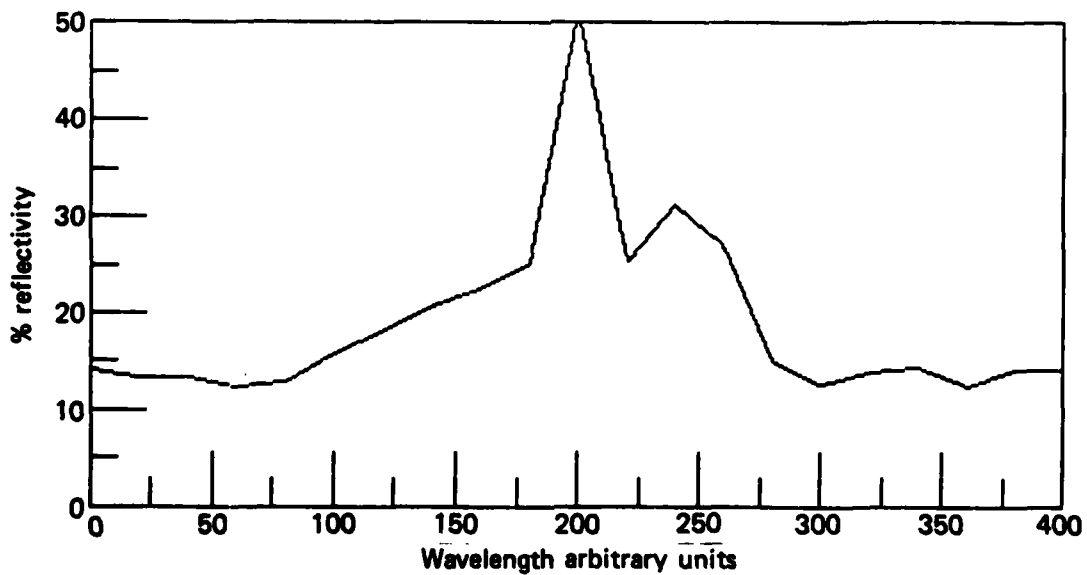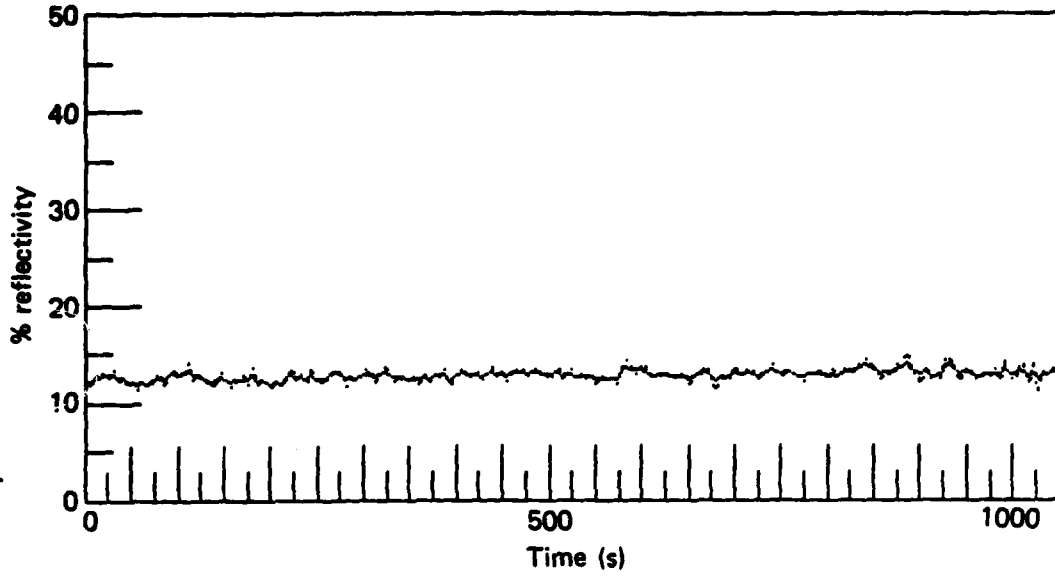Lambda is 462 nm
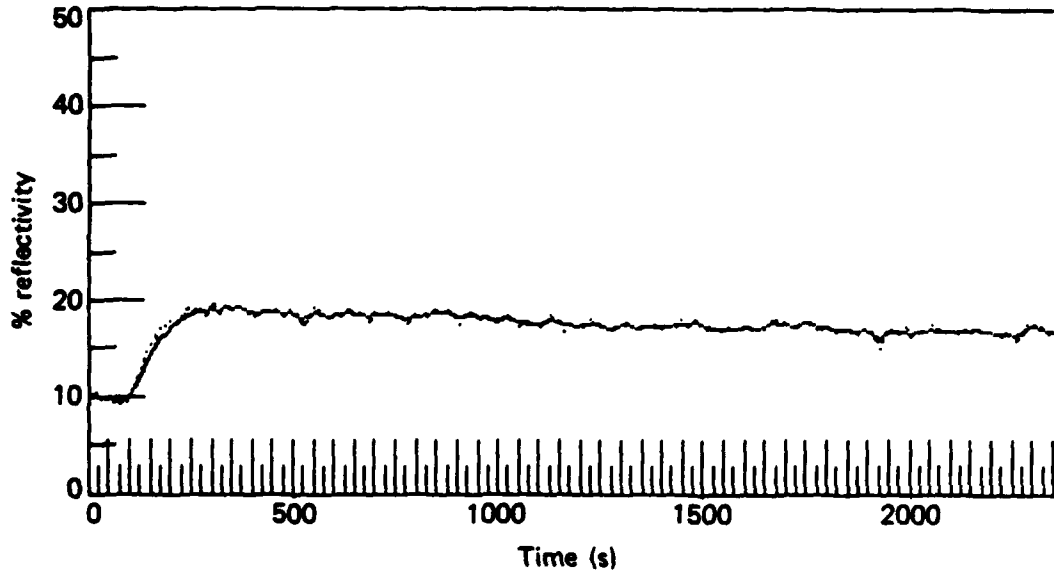
Fig. 1A

Maximum time is 2370.4 s
Lambda is 540 nm
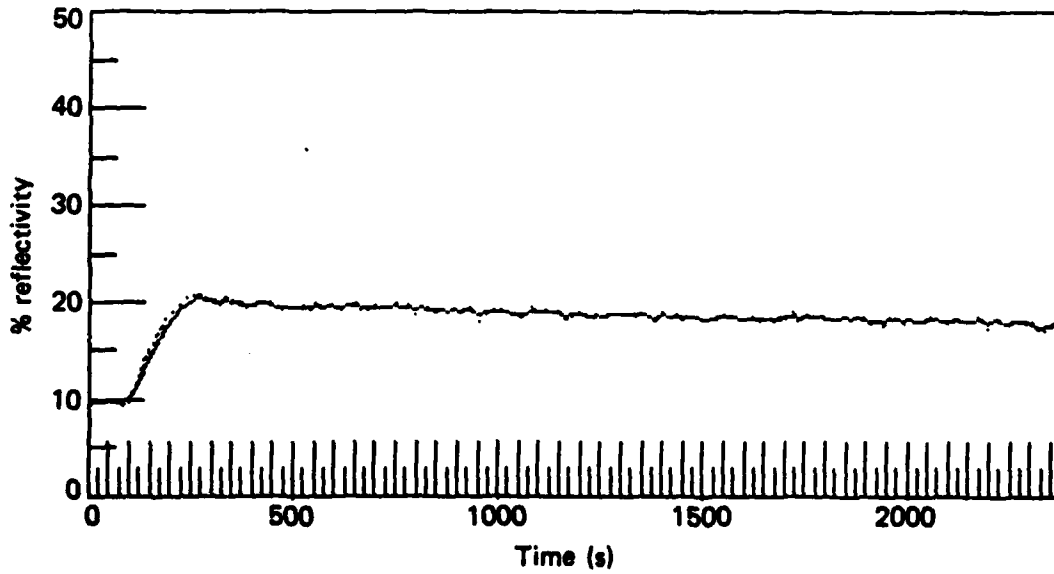
**Fig. 1B**

Maximum time is 2370.4 s
Lambda is 658 nm
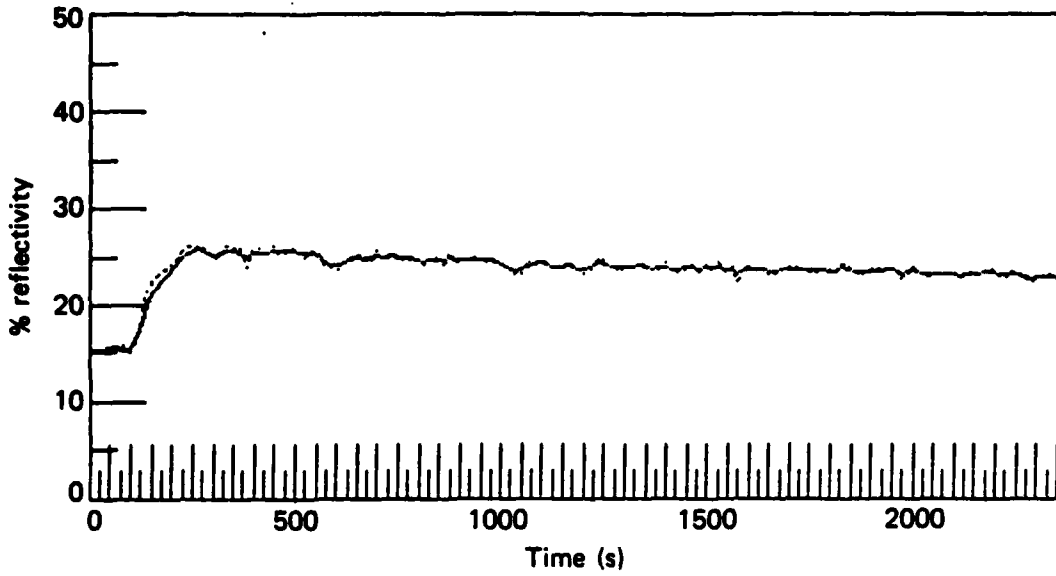
Fig. 1C

Maximum time is 2370.4 s
Lambda is 695 nm
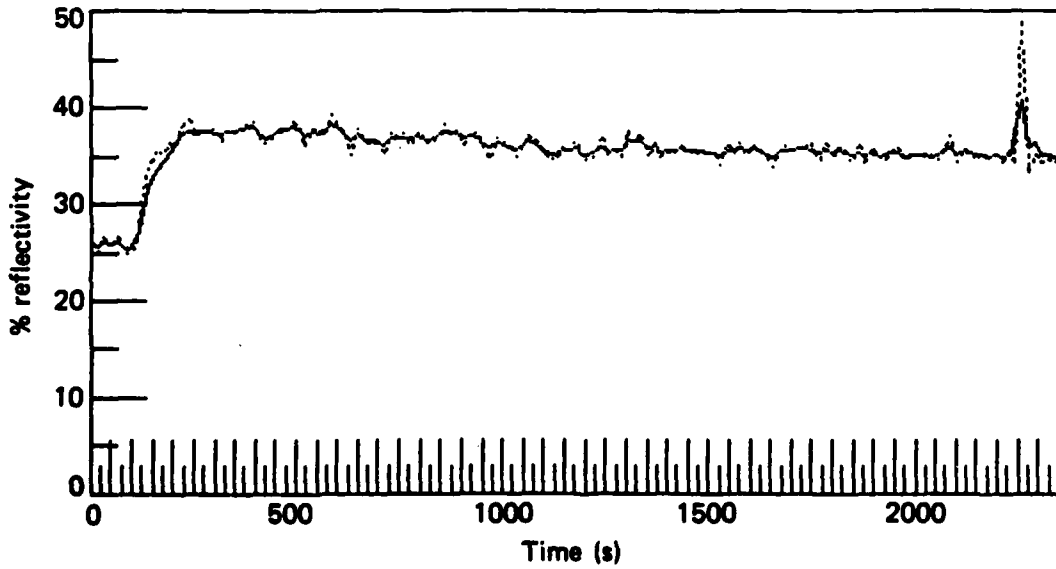
Fig. 1D

Figure 2

DATE IS

THERE WILL BE   200   SCANS

TIME DELAY BETWEEN SCANS IS   0 Sec
RUN TIME WILL BE   17.6666666667 MINUTES
SIGNAL LEVELS FROM STANDARD ARE

.04087	.04372	.04846	.05099
.10528	.93819	.98578	.93477
.82208	.55451	.05101	1.09997
.29215	.06659	.04281	.04667
.04202	.04061	.04363	.04511

REFLECTIVITY OF STANDARD IS   10 %
SHUTTER NOT USED

SCAN NO	1	TIME	0	.10021
SCAN NO	2	TIME	5.3	.1017
SCAN NO	3	TIME	10.6	.1099
SCAN NO	4	TIME	15.9	.10667
SCAN NO	5	TIME	21.2	.1129
SCAN NO	6	TIME	26.5	.65783
SCAN NO	7	TIME	31.8	.52885
SCAN NO	8	TIME	37.1	.4833
SCAN NO	9	TIME	42.4	.4598
SCAN NO	10	TIME	47.7	.44918
SCAN NO	11	TIME	53	.4327
SCAN NO	12	TIME	58.3	.39478
SCAN NO	13	TIME	63.6	.39773
SCAN NO	14	TIME	68.9	.3715
SCAN NO	15	TIME	74.2	.37182
SCAN NO	16	TIME	79.5	.37116
SCAN NO	17	TIME	84.8	.37081
SCAN NO	18	TIME	90.1	.35694
SCAN NO	19	TIME	95.4	.34834
SCAN NO	20	TIME	100.7	.33987
SCAN NO	21	TIME	106	.34969
SCAN NO	22	TIME	111.3	.34876
SCAN NO	23	TIME	116.6	.14271
SCAN NO	24	TIME	121.9	.13725
SCAN NO	25	TIME	127.2	.14525
SCAN NO	26	TIME	132.5	.14418
SCAN NO	27	TIME	137.8	.13309
SCAN NO	28	TIME	143.1	.13696
SCAN NO	29	TIME	148.4	.14452
SCAN NO	30	TIME	153.7	.13076
SCAN NO	31	TIME	159	.13456
SCAN NO	32	TIME	164.3	.13338
SCAN NO	33	TIME	169.6	.13284
SCAN NO	34	TIME	174.9	.14611
SCAN NO	35	TIME	180.2	.13361
SCAN NO	36	TIME	185.5	.12981
SCAN NO	37	TIME	190.8	.13981
SCAN NO	38	TIME	196.1	.12932
SCAN NO	39	TIME	201.4	.12896
SCAN NO	40	TIME	206.7	.13145
SCAN NO	41	TIME	212	.13282
SCAN NO	42	TIME	217.3	.13572
SCAN NO	43	TIME	222.6	.1364

Short lambda .571 DIV/nm, long lambda .34 DIV/nm
546.1 nm is at 118 divisions, 200 divisions is 660 nm
Scan time is 0
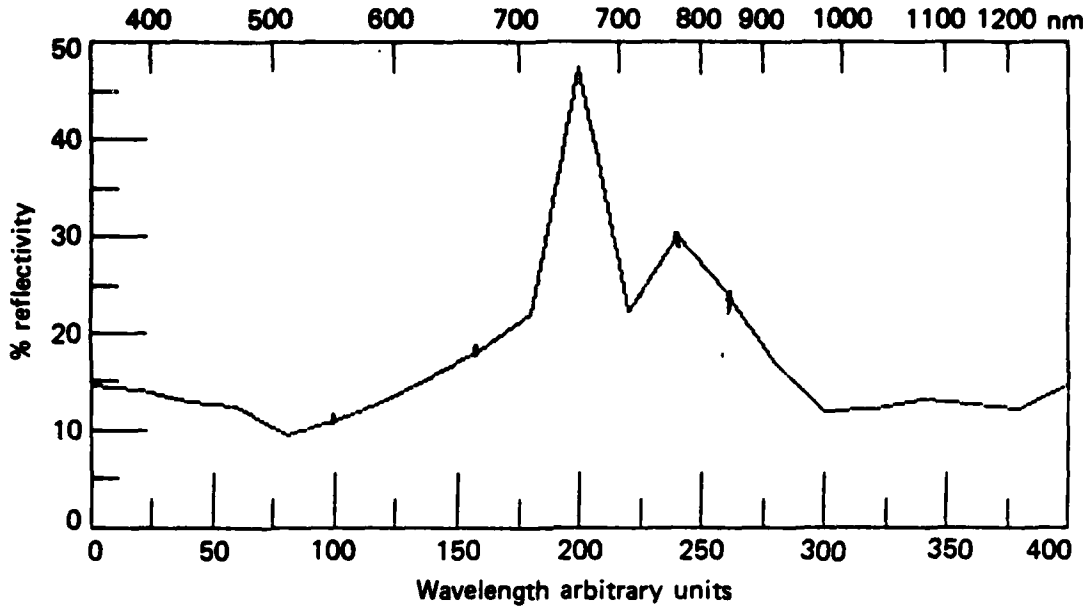
Fig. 3A

Scan time is 106
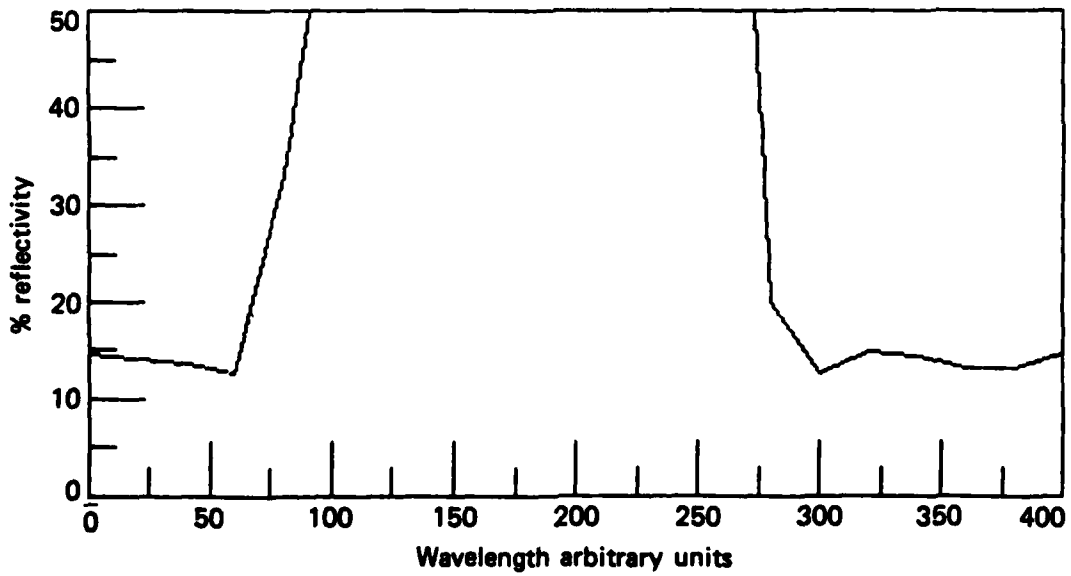
Fig. 3B

Scan time is 424.1
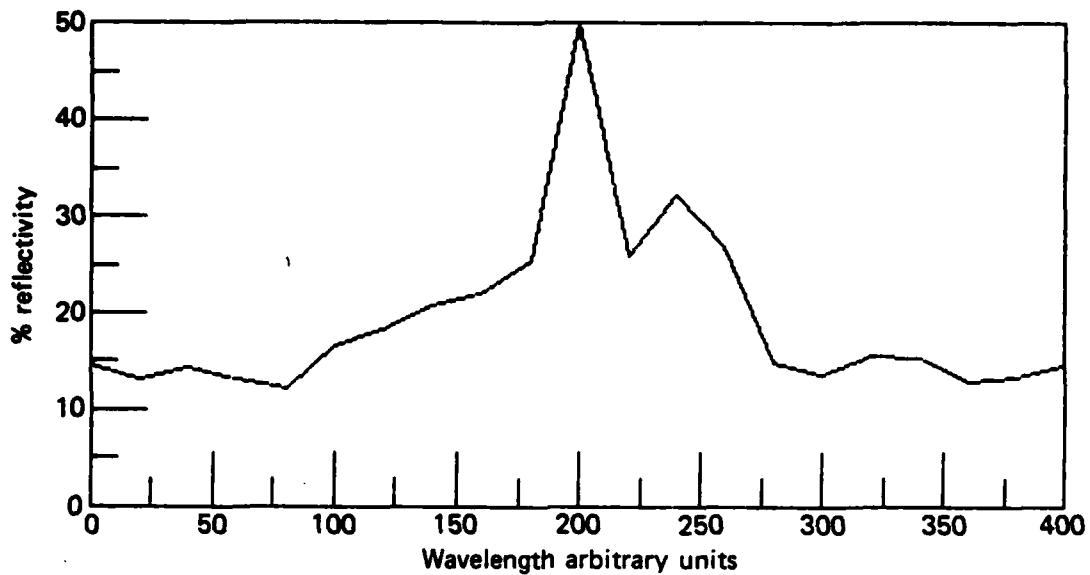
Fig. 4A

Scan time is 530.1

Fig. 4B

Maximum time is 1054.7 s
Lambda is 462 nm

Fig. 5A

Maximum time is 1054.7 s
Lambda is 540 nm
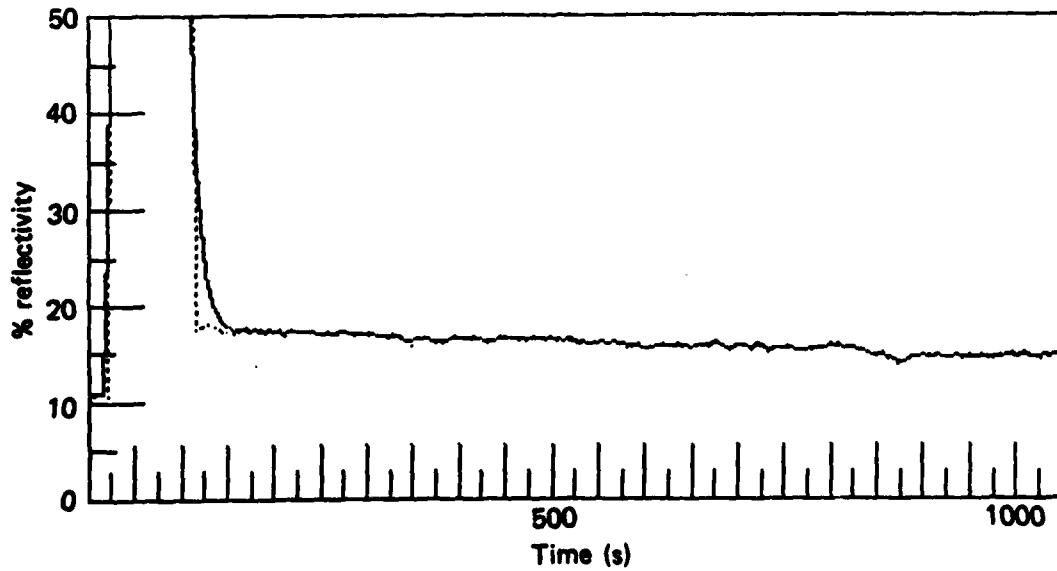
Fig. 5B

Maximum time is 1054.7 s
Lambda is 658 nm
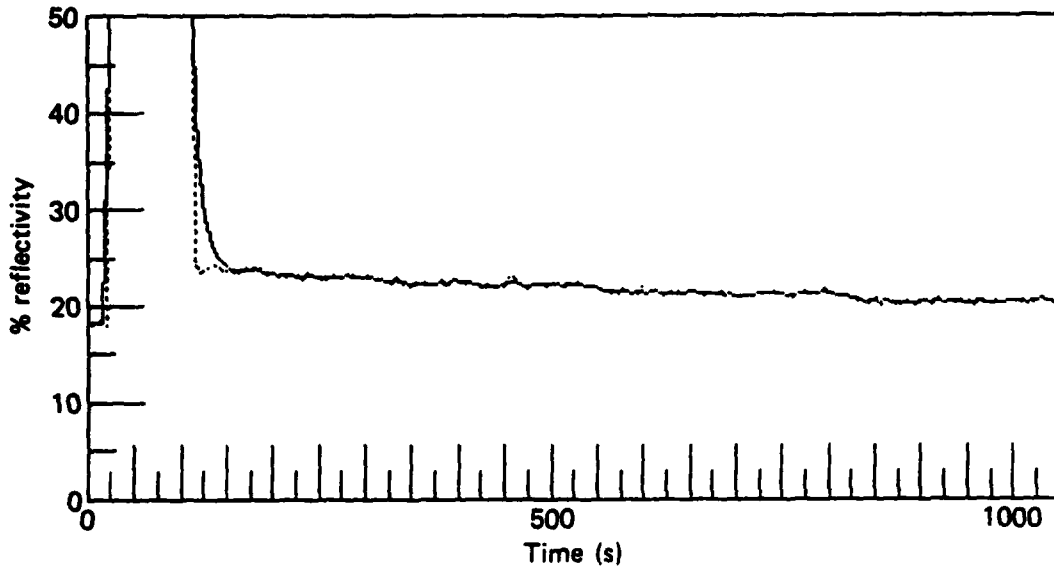
Fig. 6A

Maximum time is 1054.7 s
Lambda is 760 nm
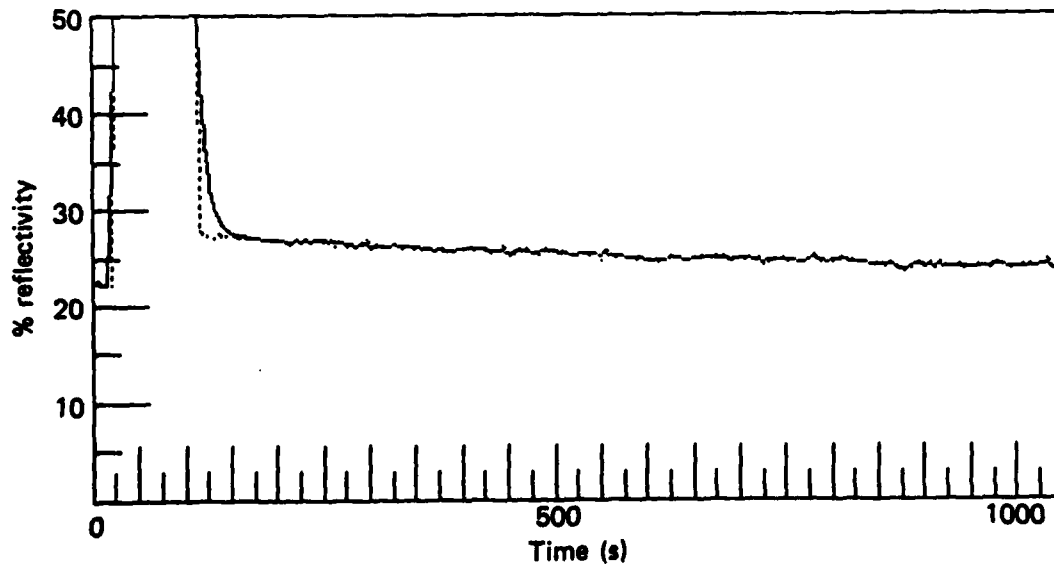
Fig. 6B

Maximum time is 1184.8 s
Lambda is 462 nm
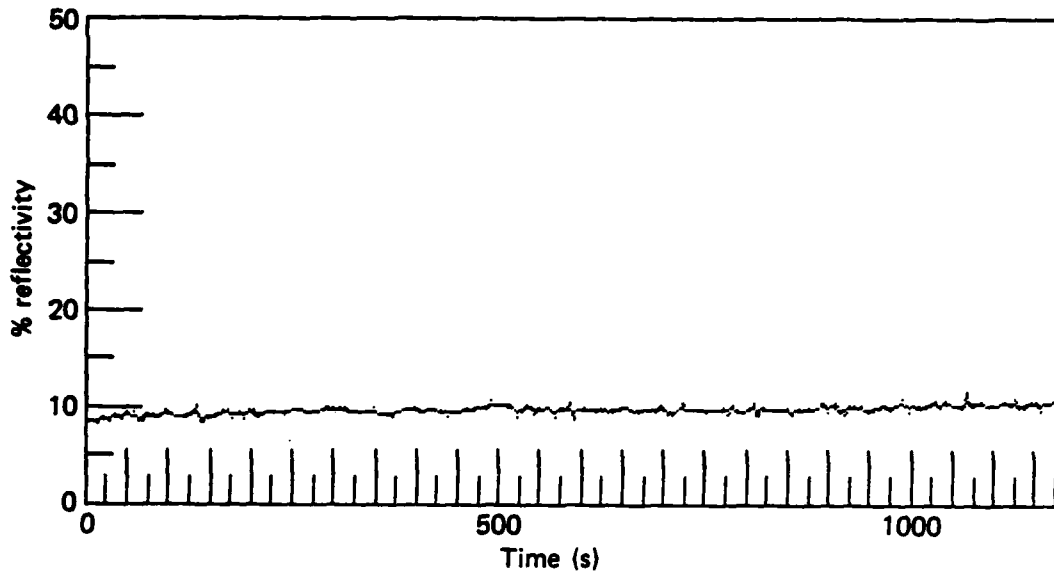
Fig. 7A

Maximum time is 1184.8 s
Lambda is 540 nm
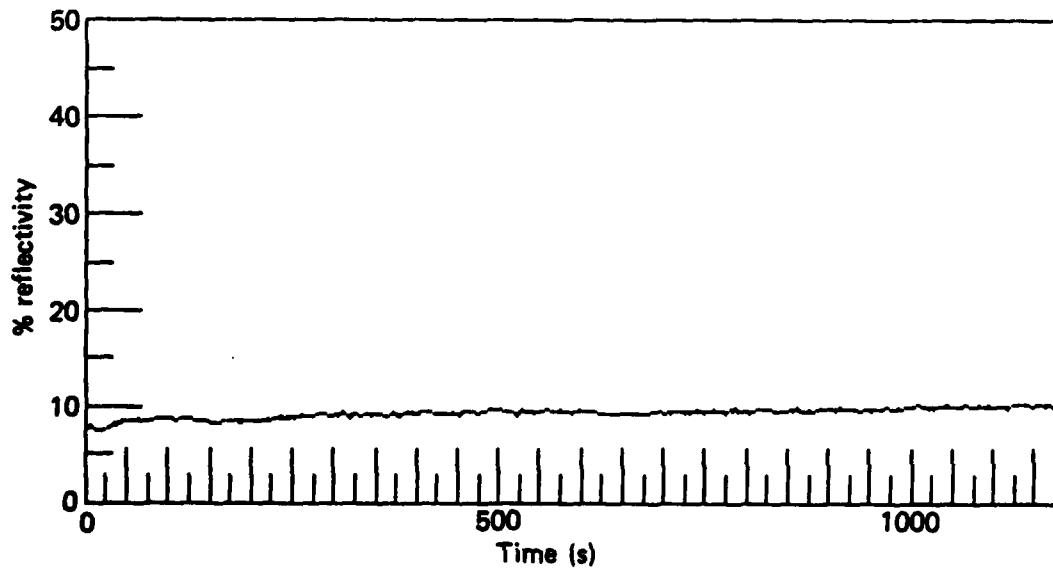
Fig. 7B

Maximum time is 1184.8 s
Lambda is 658 nm
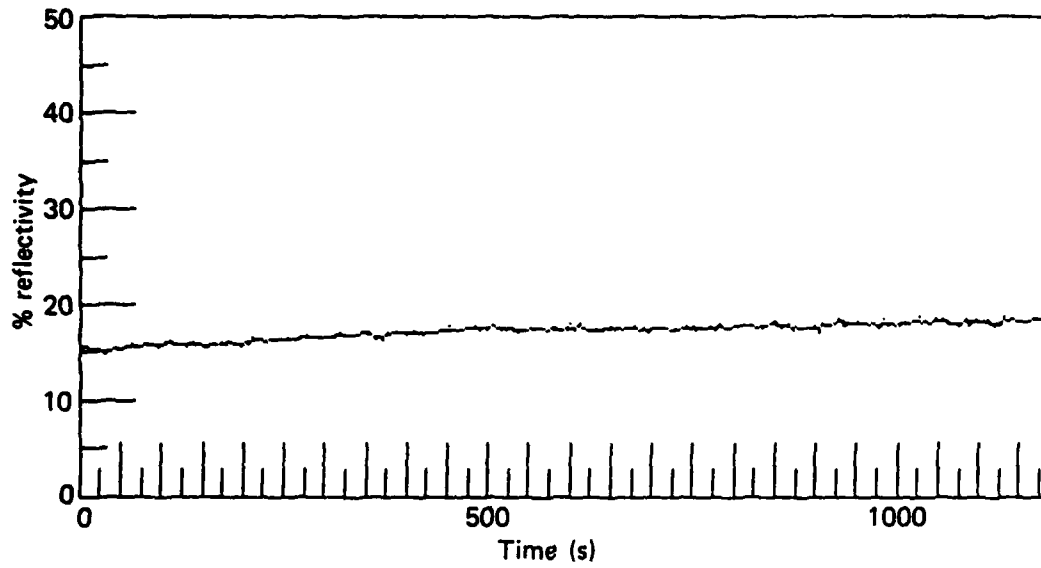
Fig. 7C

Maximum time is 1184.8 s
Lambda is 695 nm
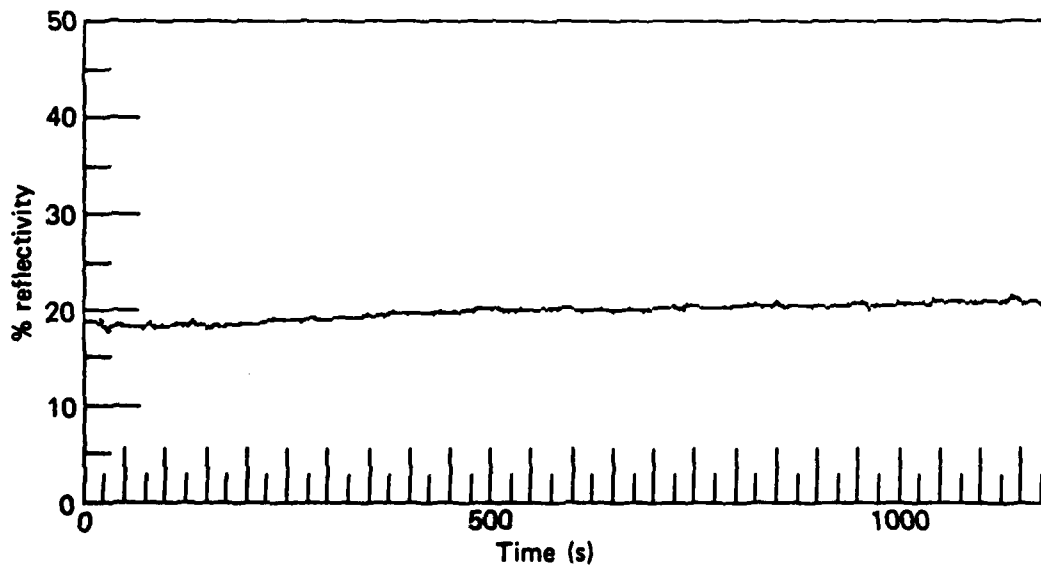
Fig. 7D

Trend 462 nm
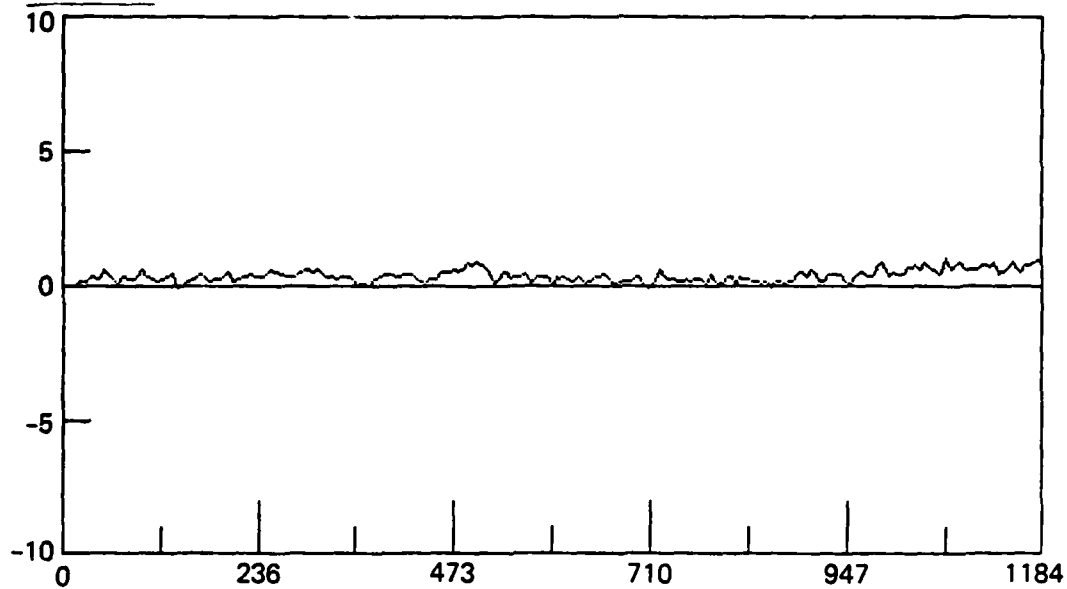
Fig. 8A

Trend 540 nm
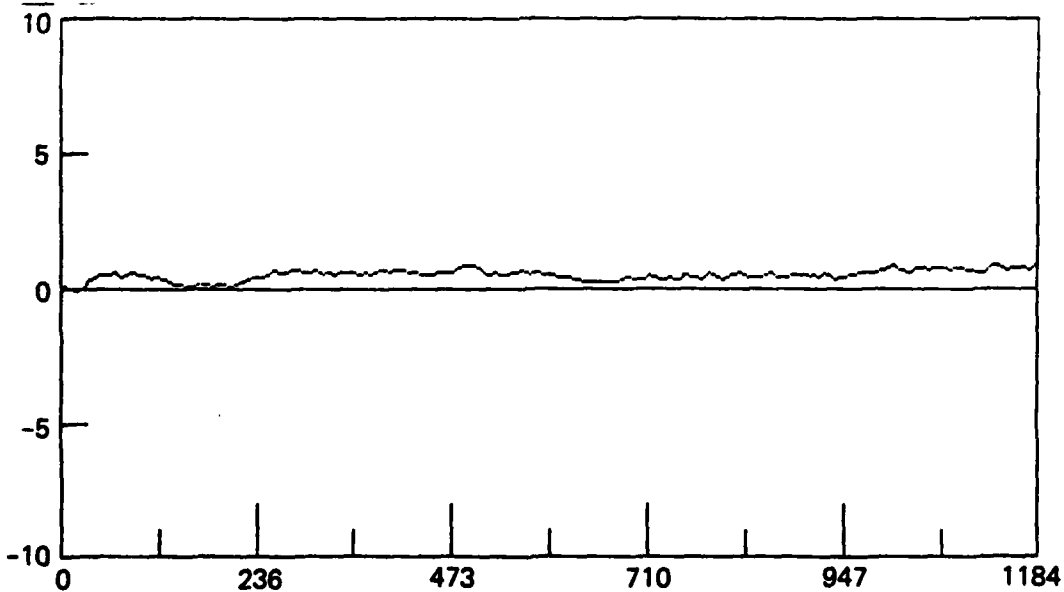
Fig. 8B

Trend 658 nm
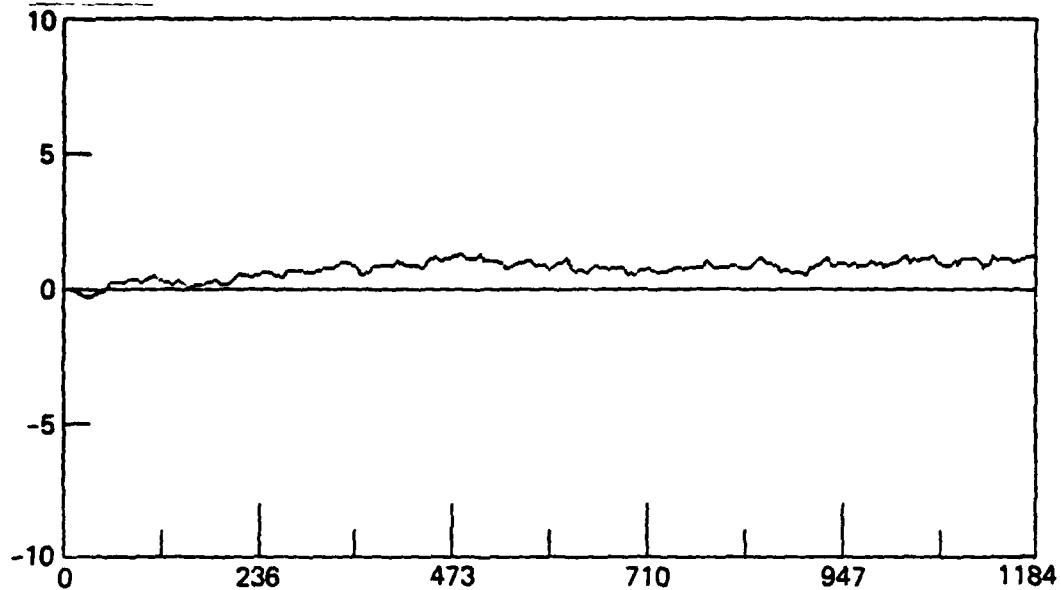
Fig. 8C

Trend 695 nm
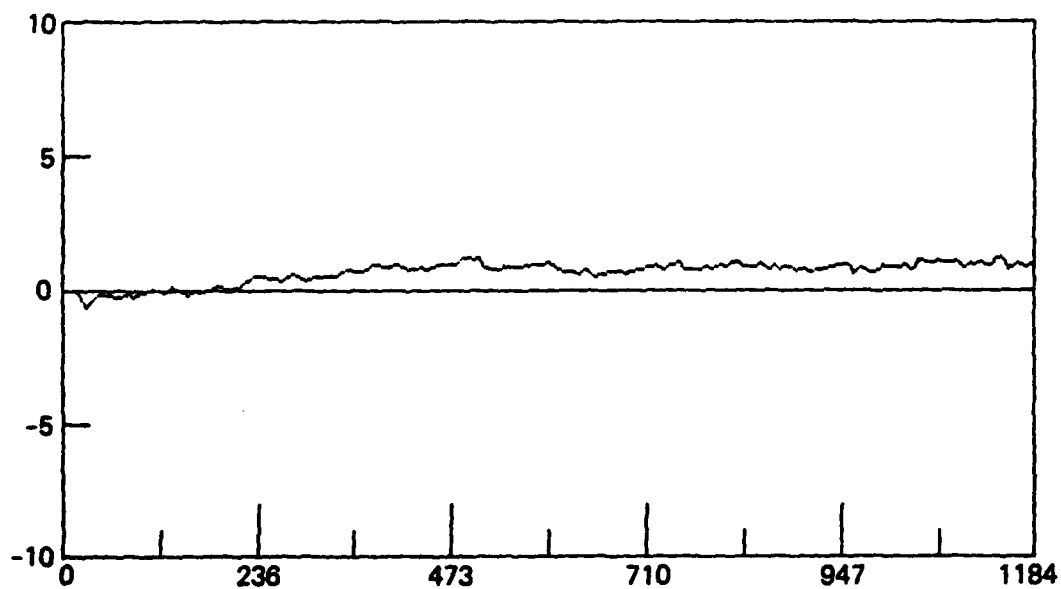
Fig. 8D

Figure 9A

```
Scan 1.00E+00  1.22E+01  1.13E+01  1.21E+01  8.50E+00  8.42E+00
Scan 6.00E+00  1.08E+01  1.18E+01  1.22E+01  8.68E+00  8.19E+00
Scan 1.10E+01  1.29E+01  1.15E+01  1.29E+01  8.80E+00  8.66E+00
Scan 1.60E+01  1.28E+01  1.06E+01  1.30E+01  9.21E+00  8.60E+00
Scan 2.10E+01  1.11E+01  1.14E+01  1.21E+01  8.84E+00  8.77E+00
Scan 2.60E+01  1.17E+01  1.28E+01  1.28E+01  9.13E+00  8.63E+00
Scan 3.10E+01  1.18E+01  1.16E+01  1.29E+01  9.26E+00  8.89E+00
Scan 3.60E+01  1.23E+01  1.16E+01  1.41E+01  9.72E+00  9.17E+00
Scan 4.10E+01  1.26E+01  1.12E+01  1.20E+01  9.69E+00  9.31E+00
Scan 4.60E+01  1.22E+01  1.09E+01  1.32E+01  9.50E+00  9.09E+00
Scan 5.10E+01  1.24E+01  1.06E+01  1.31E+01  9.27E+00  9.23E+00
Scan 5.60E+01  1.23E+01  1.16E+01  1.26E+01  9.69E+00  9.66E+00
Scan 6.10E+01  1.13E+01  1.22E+01  1.29E+01  9.36E+00  9.47E+00
Scan 6.60E+01  1.14E+01  1.15E+01  1.23E+01  9.95E+00  9.68E+00
Scan 7.10E+01  1.17E+01  1.15E+01  1.35E+01  1.02E+01  9.61E+00
Scan 7.60E+01  1.13E+01  1.16E+01  1.41E+01  9.64E+00  9.87E+00
Scan 8.10E+01  1.33E+01  1.13E+01  1.31E+01  9.78E+00  9.79E+00
Scan 8.60E+01  1.14E+01  1.15E+01  1.35E+01  9.75E+00  9.71E+00
Scan 9.10E+01  1.22E+01  1.06E+01  1.33E+01  9.81E+00  9.37E+00
Scan 9.60E+01  1.18E+01  1.09E+01  1.28E+01  9.52E+00  9.32E+00
Scan 1.01E+02  1.15E+01  1.29E+01  1.19E+01  9.75E+00  9.03E+00
Scan 1.06E+02  1.13E+01  1.25E+01  1.21E+01  9.64E+00  9.59E+00
Scan 1.11E+02  1.20E+01  1.12E+01  1.39E+01  9.58E+00  9.70E+00
Scan 1.16E+02  1.10E+01  1.15E+01  1.30E+01  9.79E+00  9.75E+00
Scan 1.21E+02  1.14E+01  1.05E+01  1.34E+01  9.80E+00  9.82E+00
Scan 1.26E+02  1.31E+01  1.24E+01  1.30E+01  9.58E+00  9.83E+00
Scan 1.31E+02  1.14E+01  1.14E+01  1.32E+01  9.84E+00  9.88E+00
Scan 1.36E+02  1.10E+01  1.17E+01  1.32E+01  9.66E+00  9.78E+00
Scan 1.41E+02  1.30E+01  1.14E+01  1.29E+01  9.60E+00  9.64E+00
Scan 1.46E+02  1.21E+01  1.20E+01  1.39E+01  9.87E+00  9.94E+00
Scan 1.51E+02  1.20E+01  1.20E+01  1.31E+01  9.97E+00  9.67E+00
Scan 1.56E+02  1.24E+01  1.11E+01  1.46E+01  9.70E+00  1.01E+01
Scan 1.61E+02  1.20E+01  1.11E+01  1.28E+01  9.94E+00  9.96E+00
Scan 1.66E+02  1.31E+01  1.20E+01  1.33E+01  1.01E+01  9.93E+00
Scan 1.71E+02  1.31E+01  1.22E+01  1.34E+01  1.04E+01  1.01E+01
Scan 1.76E+02  1.10E+01  1.19E+01  1.37E+01  1.01E+01  9.77E+00
Scan 1.81E+02  1.23E+01  1.33E+01  1.29E+01  1.06E+01  1.04E+01
Scan 1.86E+02  1.30E+01  1.14E+01  1.29E+01  1.05E+01  1.03E+01
Scan 1.91E+02  1.19E+01  1.10E+01  1.46E+01  1.02E+01  1.00E+01
Scan 1.96E+02  1.31E+01  1.15E+01  1.26E+01  1.05E+01  1.01E+01


Scan 1.00E+00  7.62E+00  8.69E+00  1.24E+01  1.56E+01  1.92E+01
Scan 6.00E+00  7.75E+00  8.95E+00  1.17E+01  1.50E+01  1.76E+01
Scan 1.10E+01  8.55E+00  1.00E+01  1.30E+01  1.56E+01  1.87E+01
Scan 1.60E+01  8.66E+00  9.92E+00  1.35E+01  1.59E+01  1.84E+01
Scan 2.10E+01  8.47E+00  9.87E+00  1.27E+01  1.59E+01  1.87E+01
Scan 2.60E+01  8.48E+00  9.63E+00  1.35E+01  1.59E+01  1.89E+01
Scan 3.10E+01  8.51E+00  9.66E+00  1.33E+01  1.63E+01  1.88E+01
Scan 3.60E+01  8.91E+00  1.01E+01  1.35E+01  1.64E+01  1.90E+01
Scan 4.10E+01  9.14E+00  1.04E+01  1.38E+01  1.65E+01  1.91E+01
Scan 4.60E+01  9.13E+00  1.06E+01  1.40E+01  1.67E+01  1.97E+01
Scan 5.10E+01  9.10E+00  1.05E+01  1.45E+01  1.66E+01  1.99E+01
Scan 5.60E+01  9.30E+00  1.07E+01  1.41E+01  1.70E+01  1.98E+01
Scan 6.10E+01  9.27E+00  1.09E+01  1.41E+01  1.70E+01  1.99E+01
Scan 6.60E+01  9.34E+00  1.11E+01  1.45E+01  1.75E+01  2.06E+01
Scan 7.10E+01  9.67E+00  1.12E+01  1.47E+01  1.75E+01  2.06E+01
Scan 7.60E+01  9.50E+00  1.08E+01  1.44E+01  1.75E+01  2.03E+01
Scan 8.10E+01  9.53E+00  1.09E+01  1.47E+01  1.75E+01  2.00E+01
Scan 8.60E+01  9.54E+00  1.07E+01  1.48E+01  1.75E+01  2.04E+01
```

Figure 9B

```
Scan 9.10E+01   9.42E+00   1.08E+01   1.45E+01   1.76E+01   1.97E+01
Scan 9.60E+01   9.25E+00   1.07E+01   1.44E+01   1.73E+01   2.05E+01
Scan 1.01E+02   9.25E+00   1.08E+01   1.43E+01   1.75E+01   2.00E+01
Scan 1.06E+02   9.43E+00   1.12E+01   1.49E+01   1.73E+01   2.01E+01
Scan 1.11E+02   9.51E+00   1.08E+01   1.48E+01   1.75E+01   2.03E+01
Scan 1.16E+02   9.49E+00   1.08E+01   1.45E+01   1.75E+01   2.07E+01
Scan 1.21E+02   9.49E+00   1.09E+01   1.46E+01   1.76E+01   1.98E+01
Scan 1.26E+02   9.57E+00   1.08E+01   1.49E+01   1.76E+01   2.07E+01
Scan 1.31E+02   9.65E+00   1.09E+01   1.49E+01   1.78E+01   2.06E+01
Scan 1.36E+02   9.53E+00   1.10E+01   1.49E+01   1.80E+01   2.11E+01
Scan 1.41E+02   9.53E+00   1.13E+01   1.48E+01   1.76E+01   2.13E+01
Scan 1.46E+02   9.66E+00   1.12E+01   1.48E+01   1.75E+01   2.06E+01
Scan 1.51E+02   9.74E+00   1.12E+01   1.47E+01   1.80E+01   2.12E+01
Scan 1.56E+02   9.62E+00   1.10E+01   1.49E+01   1.80E+01   2.07E+01
Scan 1.61E+02   9.77E+00   1.11E+01   1.49E+01   1.79E+01   2.11E+01
Scan 1.66E+02   1.00E+01   1.12E+01   1.48E+01   1.79E+01   2.12E+01
Scan 1.71E+02   9.87E+00   1.17E+01   1.49E+01   1.81E+01   2.10E+01
Scan 1.76E+02   1.00E+01   1.13E+01   1.52E+01   1.84E+01   2.10E+01
Scan 1.81E+02   1.00E+01   1.12E+01   1.55E+01   1.83E+01   2.13E+01
Scan 1.86E+02   9.96E+00   1.16E+01   1.50E+01   1.84E+01   2.11E+01
Scan 1.91E+02   1.02E+01   1.16E+01   1.51E+01   1.83E+01   2.11E+01
Scan 1.96E+02   1.01E+01   1.15E+01   1.51E+01   1.83E+01   2.12E+01


Scan 1.00E+00   3.75E+01   1.89E+01   2.89E+01   2.71E+01   1.10E+01
Scan 6.00E+00   3.65E+01   1.80E+01   2.66E+01   2.64E+01   1.26E+01
Scan 1.10E+01   3.49E+01   1.83E+01   2.77E+01   2.53E+01   1.24E+01
Scan 1.60E+01   3.64E+01   1.84E+01   2.68E+01   2.57E+01   1.19E+01
Scan 2.10E+01   3.72E+01   1.85E+01   2.73E+01   2.54E+01   1.21E+01
Scan 2.60E+01   3.59E+01   1.84E+01   2.69E+01   2.57E+01   1.28E+01
Scan 3.10E+01   3.84E+01   1.86E+01   2.67E+01   2.54E+01   1.39E+01
Scan 3.60E+01   3.84E+01   1.90E+01   2.65E+01   2.58E+01   1.26E+01
Scan 4.10E+01   4.02E+01   1.91E+01   2.66E+01   2.54E+01   1.20E+01
Scan 4.60E+01   3.55E+01   1.92E+01   2.72E+01   2.57E+01   1.27E+01
Scan 5.10E+01   3.64E+01   1.94E+01   2.65E+01   2.50E+01   1.29E+01
Scan 5.60E+01   3.59E+01   1.97E+01   2.79E+01   2.53E+01   1.28E+01
Scan 6.10E+01   3.95E+01   1.97E+01   2.83E+01   2.58E+01   1.40E+01
Scan 6.60E+01   3.84E+01   1.99E+01   2.79E+01   2.52E+01   1.26E+01
Scan 7.10E+01   3.75E+01   2.02E+01   2.81E+01   2.62E+01   1.14E+01
Scan 7.60E+01   3.73E+01   1.99E+01   2.67E+01   2.57E+01   1.24E+01
Scan 8.10E+01   3.80E+01   2.00E+01   2.76E+01   2.58E+01   1.28E+01
Scan 8.60E+01   3.68E+01   2.01E+01   2.84E+01   2.53E+01   1.24E+01
Scan 9.10E+01   3.89E+01   2.00E+01   2.81E+01   2.55E+01   1.18E+01
Scan 9.60E+01   3.75E+01   2.00E+01   2.68E+01   2.61E+01   1.11E+01
Scan 1.01E+02   3.90E+01   2.00E+01   2.81E+01   2.62E+01   1.18E+01
Scan 1.06E+02   3.84E+01   2.00E+01   2.83E+01   2.59E+01   1.24E+01
Scan 1.11E+02   4.21E+01   2.02E+01   2.78E+01   2.52E+01   1.21E+01
Scan 1.16E+02   3.88E+01   2.04E+01   2.96E+01   2.60E+01   1.22E+01
Scan 1.21E+02   4.09E+01   2.03E+01   2.76E+01   2.52E+01   1.26E+01
Scan 1.26E+02   3.91E+01   2.03E+01   2.77E+01   2.59E+01   1.23E+01
Scan 1.31E+02   3.82E+01   2.06E+01   2.84E+01   2.66E+01   1.22E+01
Scan 1.36E+02   4.04E+01   2.04E+01   2.78E+01   2.56E+01   1.27E+01
Scan 1.41E+02   3.83E+01   2.04E+01   2.84E+01   2.52E+01   1.23E+01
Scan 1.46E+02   3.89E+01   2.05E+01   2.80E+01   2.59E+01   1.37E+01
Scan 1.51E+02   4.04E+01   2.04E+01   2.88E+01   2.61E+01   1.29E+01
Scan 1.56E+02   3.92E+01   2.07E+01   2.89E+01   2.64E+01   1.20E+01
Scan 1.61E+02   4.00E+01   2.05E+01   2.83E+01   2.65E+01   1.28E+01
Scan 1.66E+02   3.77E+01   2.06E+01   2.67E+01   2.58E+01   1.27E+01
Scan 1.71E+02   3.76E+01   2.06E+01   2.88E+01   2.62E+01   1.28E+01
Scan 1.76E+02   3.77E+01   2.08E+01   2.84E+01   2.65E+01   1.20E+01
Scan 1.81E+02   3.79E+01   2.08E+01   2.78E+01   2.62E+01   1.27E+01
Scan 1.86E+02   3.95E+01   2.09E+01   2.91E+01   2.63E+01   1.27E+01
Scan 1.91E+02   3.85E+01   2.12E+01   2.92E+01   2.61E+01   1.21E+01
Scan 1.96E+02   4.03E+01   2.10E+01   2.89E+01   2.66E+01   1.18E+01
```

Figure 9C

```
Scan 1.00E+00  1.27E+01  1.57E+01  1.19E+01  1.04E+01  1.19E+01
Scan 6.00E+00  1.25E+01  1.32E+01  1.40E+01  1.18E+01  1.15E+01
Scan 1.10E+01  1.30E+01  1.31E+01  1.34E+01  1.10E+01  1.13E+01
Scan 1.60E+01  1.20E+01  1.33E+01  1.29E+01  1.27E+01  1.09E+01
Scan 2.10E+01  1.27E+01  1.24E+01  1.17E+01  1.07E+01  1.20E+01
Scan 2.60E+01  1.27E+01  1.40E+01  1.45E+01  1.16E+01  1.10E+01
Scan 3.10E+01  1.41E+01  1.51E+01  1.30E+01  1.15E+01  1.30E+01
Scan 3.60E+01  1.27E+01  1.30E+01  1.36E+01  1.17E+01  1.29E+01
Scan 4.10E+01  1.27E+01  1.36E+01  1.33E+01  1.10E+01  1.32E+01
Scan 4.60E+01  1.25E+01  1.43E+01  1.35E+01  1.12E+01  1.11E+01
Scan 5.10E+01  1.29E+01  1.26E+01  1.39E+01  1.21E+01  1.16E+01
Scan 5.60E+01  1.33E+01  1.40E+01  1.35E+01  1.15E+01  1.18E+01
Scan 6.10E+01  1.29E+01  1.42E+01  1.31E+01  1.11E+01  1.33E+01
Scan 6.60E+01  1.29E+01  1.40E+01  1.49E+01  1.09E+01  1.26E+01
Scan 7.10E+01  1.26E+01  1.49E+01  1.32E+01  1.15E+01  1.20E+01
Scan 7.60E+01  1.26E+01  1.24E+01  1.47E+01  1.15E+01  1.31E+01
Scan 8.10E+01  1.34E+01  1.43E+01  1.33E+01  1.13E+01  1.29E+01
Scan 8.60E+01  1.29E+01  1.29E+01  1.20E+01  1.10E+01  1.21E+01
Scan 9.10E+01  1.28E+01  1.38E+01  1.34E+01  1.15E+01  1.17E+01
Scan 9.60E+01  1.29E+01  1.55E+01  1.32E+01  1.30E+01  1.25E+01
Scan 1.01E+02  1.28E+01  1.46E+01  1.35E+01  1.10E+01  1.17E+01
Scan 1.06E+02  1.32E+01  1.44E+01  1.28E+01  1.14E+01  1.26E+01
Scan 1.11E+02  1.24E+01  1.27E+01  1.54E+01  1.11E+01  1.29E+01
Scan 1.16E+02  1.32E+01  1.33E+01  1.28E+01  1.22E+01  1.23E+01
Scan 1.21E+02  1.31E+01  1.28E+01  1.40E+01  1.13E+01  1.27E+01
Scan 1.26E+02  1.26E+01  1.38E+01  1.38E+01  1.18E+01  1.32E+01
Scan 1.31E+02  1.33E+01  1.42E+01  1.39E+01  1.18E+01  1.05E+01
Scan 1.36E+02  1.30E+01  1.42E+01  1.31E+01  1.11E+01  1.22E+01
Scan 1.41E+02  1.23E+01  1.44E+01  1.39E+01  1.17E+01  1.14E+01
Scan 1.46E+02  1.29E+01  1.39E+01  1.31E+01  1.09E+01  1.14E+01
Scan 1.51E+02  1.34E+01  1.42E+01  1.34E+01  1.15E+01  1.26E+01
Scan 1.56E+02  1.25E+01  1.44E+01  1.32E+01  1.04E+01  1.18E+01
Scan 1.61E+02  1.31E+01  1.45E+01  1.23E+01  1.08E+01  1.24E+01
Scan 1.66E+02  1.31E+01  1.37E+01  1.36E+01  1.15E+01  1.21E+01
Scan 1.71E+02  1.33E+01  1.39E+01  1.36E+01  1.14E+01  1.15E+01
Scan 1.76E+02  1.34E+01  1.45E+01  1.40E+01  1.26E+01  1.31E+01
Scan 1.81E+02  1.29E+01  1.28E+01  1.38E+01  1.27E+01  1.23E+01
Scan 1.86E+02  1.38E+01  1.48E+01  1.43E+01  1.05E+01  1.24E+01
Scan 1.91E+02  1.28E+01  1.49E+01  1.36E+01  1.21E+01  1.31E+01
Scan 1.96E+02  1.30E+01  1.35E+01  1.37E+01  1.14E+01  1.17E+01
NO MULTIPROGRAMMER ERRORS
FINISHED
```

Scan time is 106
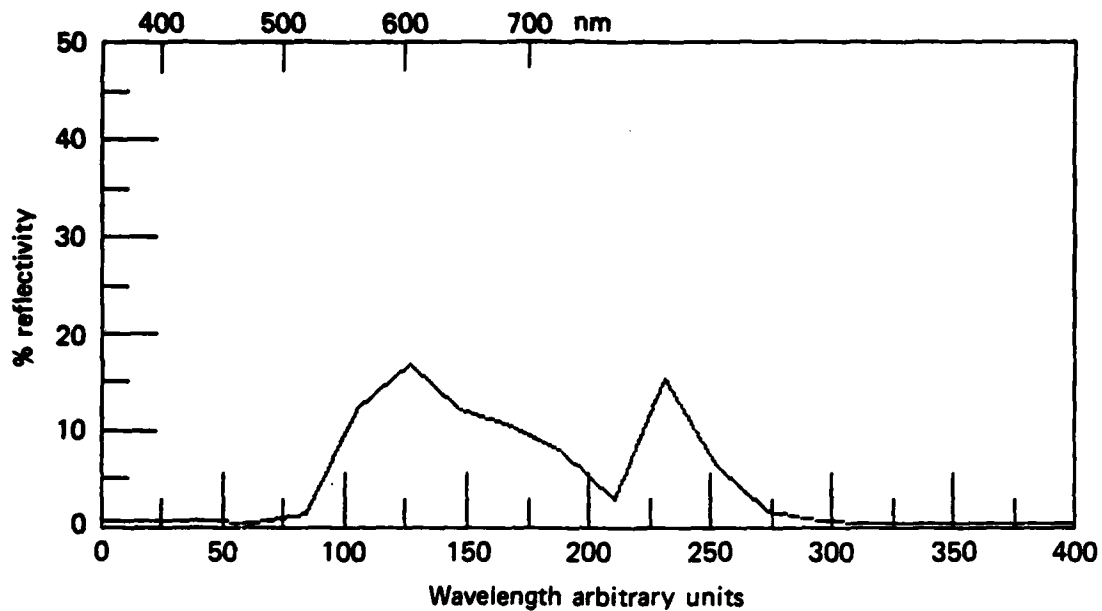
Fig. 10

Maximum time is 127.2 s
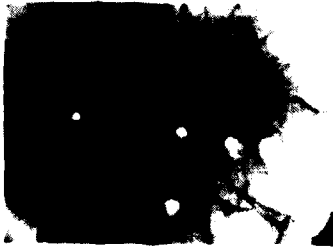**Lambda is 462 nm**
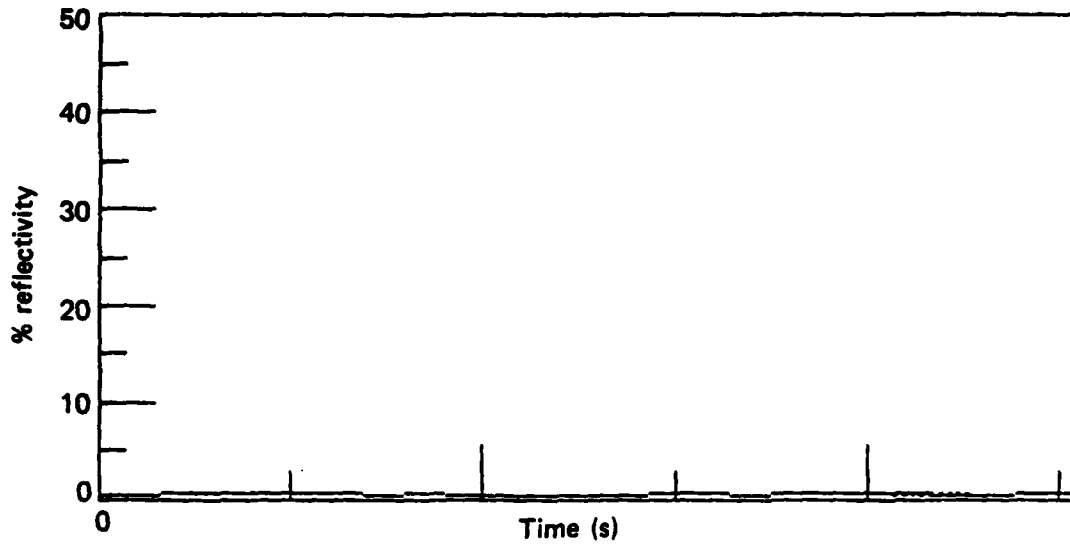
Fig. 11A

Maximum time is 127.2 s
Lambda is 540 nm
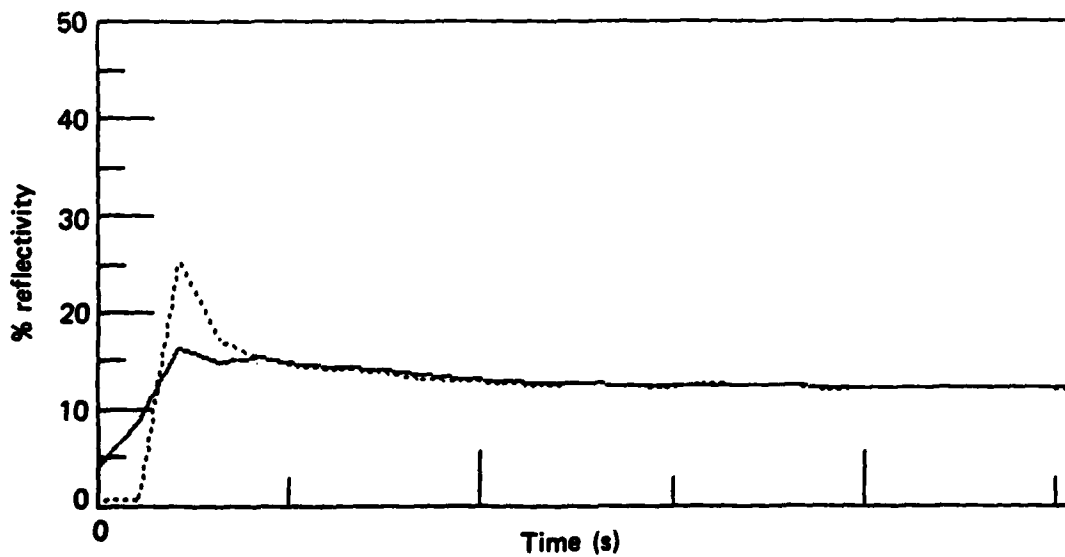
Fig. 11B

Maximum time is 127.2 s
Lambda is 658 nm
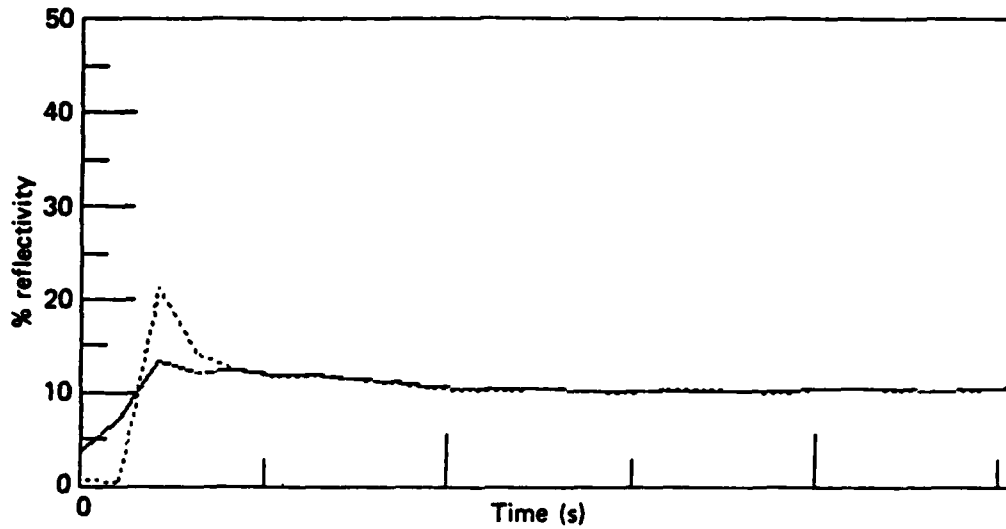
Fig. 11C

Maximum time is 127.2 s
Lambda is 695 nm
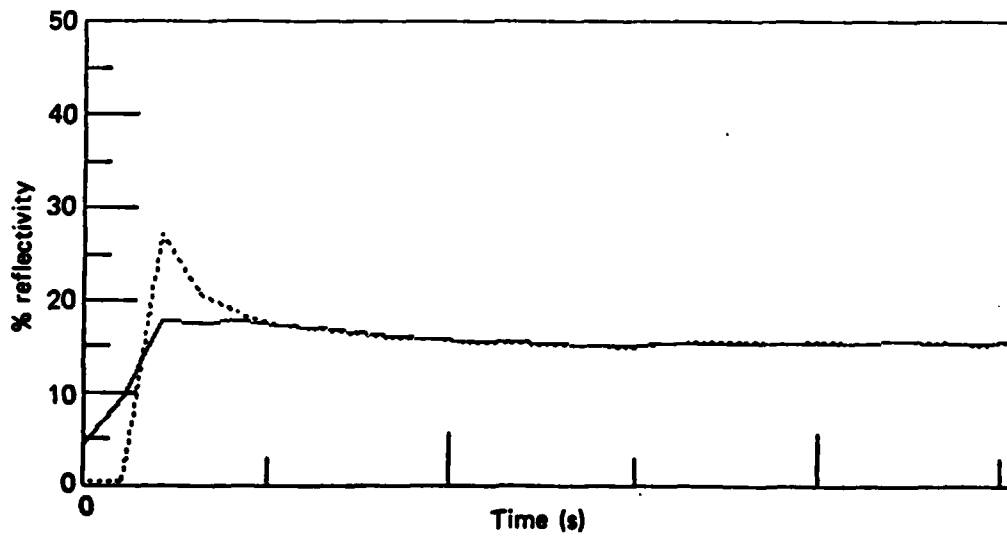
Fig. 11D

Figure 12A
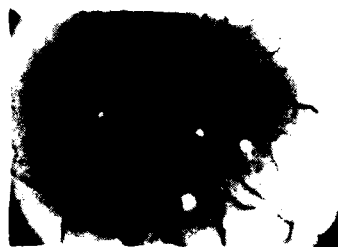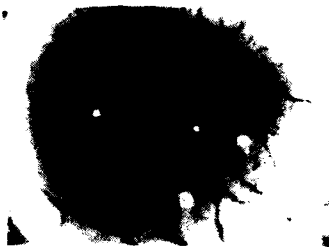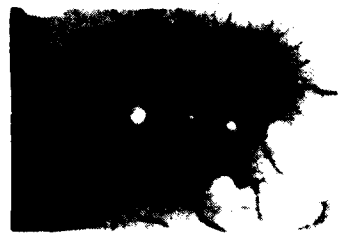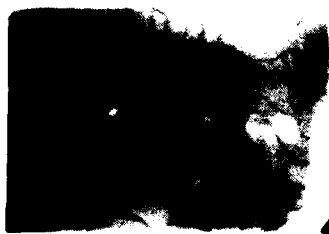
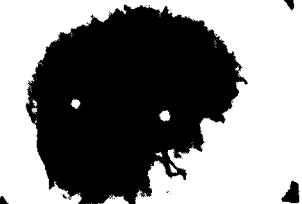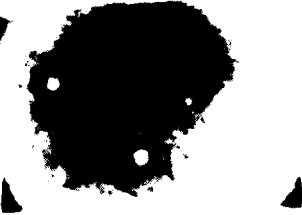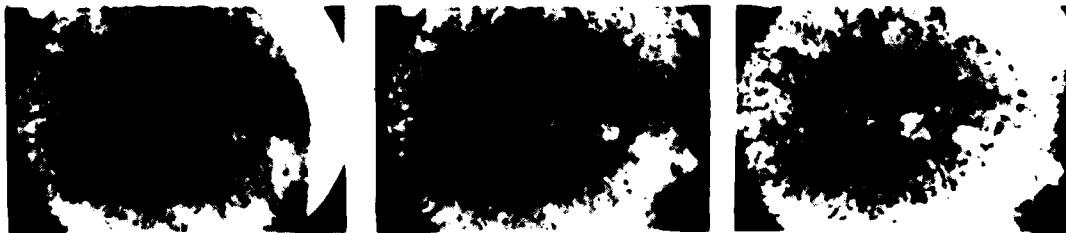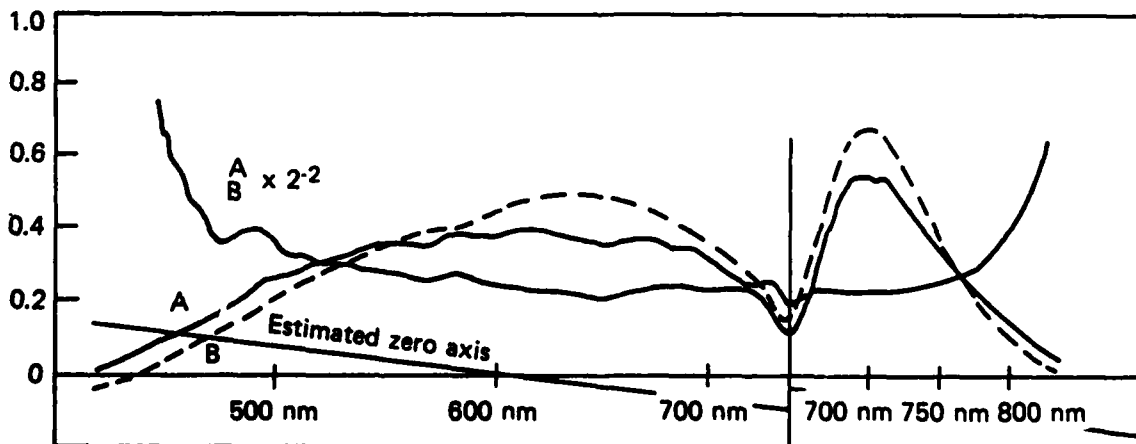| 400	450	500	
			Sept. 21
			Sept. 23
			Sept. 28
			Oct. 5
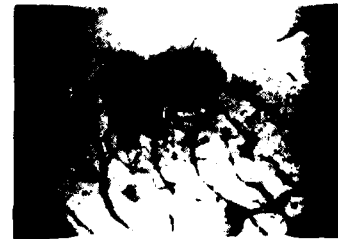
Figure 12B

550　　　　　　600　　　　　　650　　　　　　700
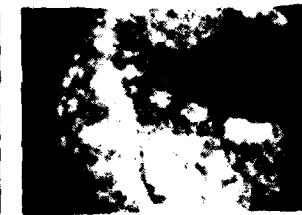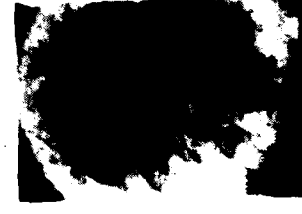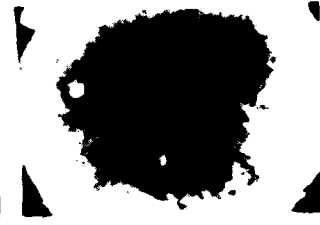
Figure 12C

750 800 850
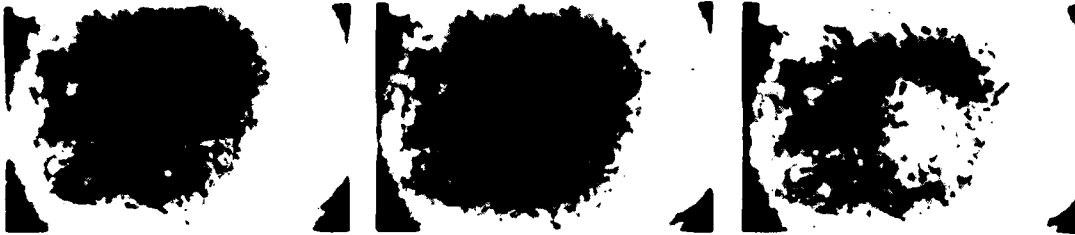
Figure 12D
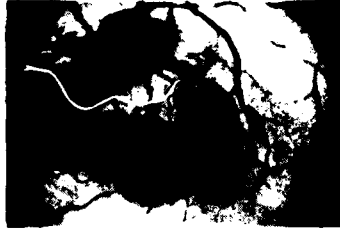
400	450	500	
			Oct. 12
			Oct. 19
			Dec. 5
			Dec. 12
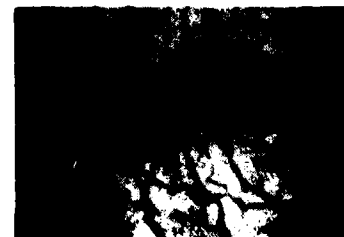
Figure 12E
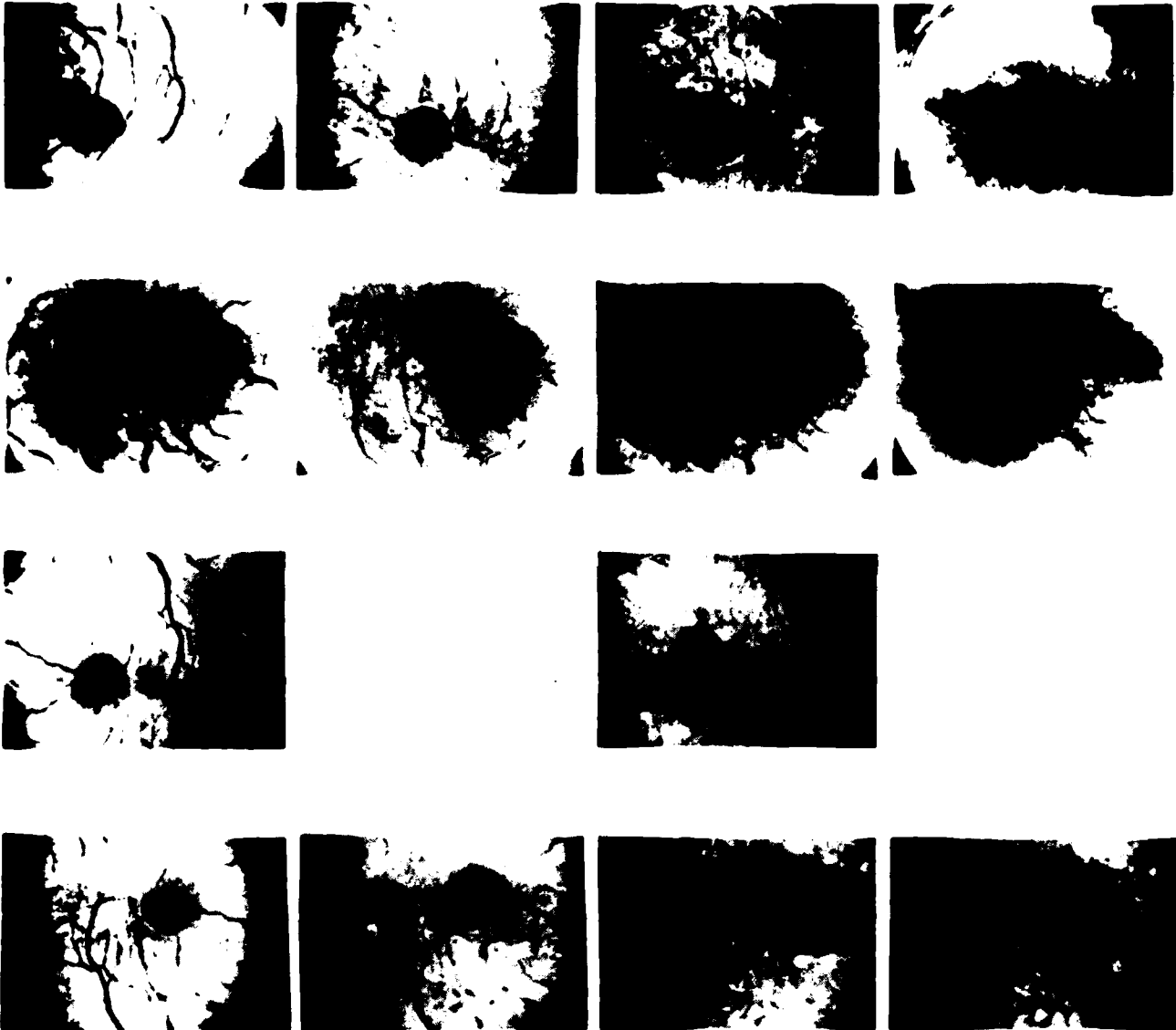
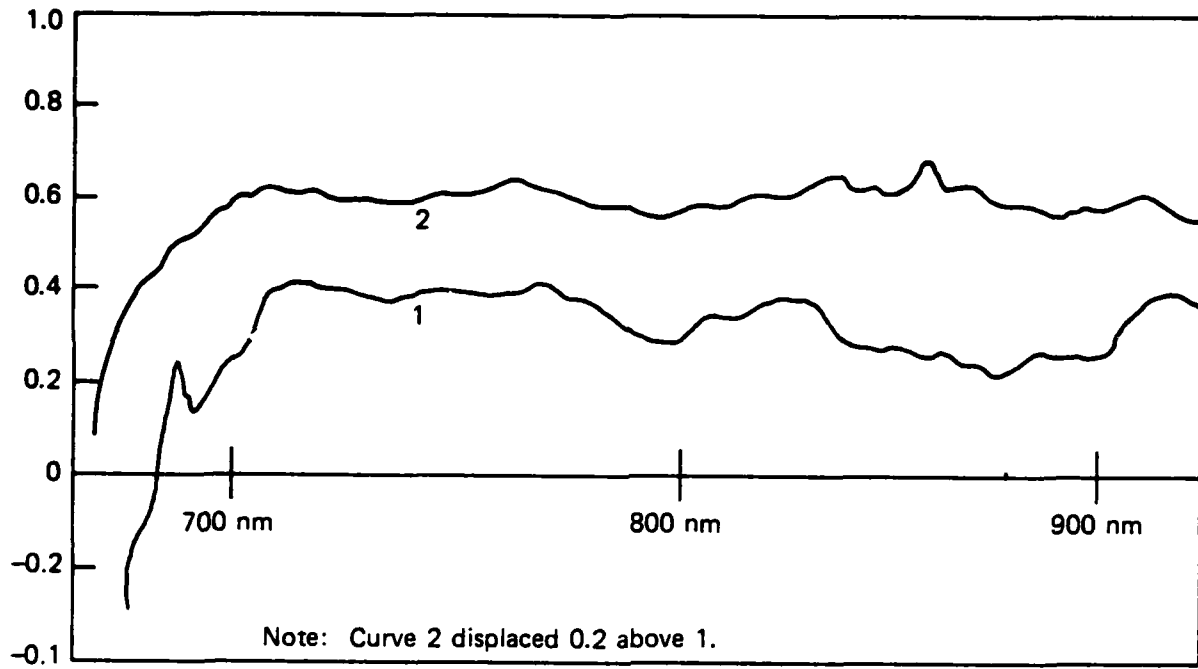Figure 12F

750   800   850

Fig. 13

Fig. 14

Note: Curve 2 displaced 0.2 above 1.

Fig. 15

Fig. 16